Distribution Agreement

In presenting this dissertation as a partial fulfillment of the requirements for an advanced degree from Emory University, I hereby grant Emory University and its agents the non-exclusive license to archive, make accessible, and display my thesis or dissertation in whole or in part in all forms of media, now or hereafter known, including display on the world wide web. I understand that I may select some access restrictions as part of the online submission of this thesis or dissertation. I retain all ownership rights to the copyright of the thesis or dissertation. I also retain to use in future works (such as articles or books) all or part of this thesis or dissertation.

Signature:

_____ _____

Qing Shao Date

DNA elasticity and effects on Type II topoisomerases

By

Qing Shao
Doctor of Philosophy

Physics

_____
Dr. David Dunlap
Advisor

_____
Dr. Laura Finzi
Advisor

_____
Dr. Fereydoon Family
Committee Member

_____
Dr. Ivan Rasnik
Committee Member

_____
Dr. Kurt Warncke
Committee Member

_____
Dr. Eric Weeks
Committee Member

Accepted:

_____
Lisa A. Tedesco, Ph.D.
Dean of the James T. Laney School of Graduate Studies

_____
Date

DNA elasticity and effects on Type II topoisomerases

By

Qing Shao
B.S., Shanghai Jiao Tong University,
China 2005

Advisor: David Dunlap, Ph.D.

Advisor: Laura Finzi, Ph.D

An abstract of
A dissertation submitted to the Faculty of the
James T. Laney Graduate School Studies of Emory University
in Partial Fulfillment of the Requirements for the Degree of
Doctor of Philosophy
in Physics
2011

Abstract

DNA elasticity and effects on Type II topoisomerases

By Qing Shao

The exceptional stiffness of DNA is routinely attributed to base pair stacking, hydrogen bonding, and electrostatic repulsion between neighboring, negatively charged phosphates. Understanding how these factors contribute to the stiffness and mechanical properties of DNA is very important to understand how cells use counterions, sequence variety as well as enzymes to manage DNA. Using Magnetic Tweezers to twist and stretch single DNA molecules, experiments were performed to probe the parameters of DNA stiffness. Experiments showed that diaminopurine (DAP) substitution for adenine, which adds an additional hydrogen bond to A:T base pairs, stiffens DNA by about 40% without significantly changing the buckling transition point. Moreover, DAP-substituted DNA fragments showed different behavior under extreme unwinding at high tension indicating sequence dependent DNA deformation and right to left hand transition. Furthermore, adding low molecular weight polycations such as spermine or spermidine to the solution appeared to soften DNA and promote plectoneme formation at lower values of torsion.

Bending a stiff polymer like DNA requires considerable energy and could represent the rate limiting step in enzymatically catalyzed processes that modify the topology of DNA. For example the activity of type II topoisomerases that catalyze DNA decatenation and unwinding which is essential for cell division might be altered. A recently published crystal structure shows that, during the catalytic cycle, a yeast type II topoisomerase can bend a 34 base pair DNA segment by up to 150 degrees. Bacterial gyrase, another type II topoisomerase, can wrap an approximately 100 bp DNA segment into a tight 180 degree turn. To test whether or not DNA stiffness modifies topoisomerase activity, DAP DNA has been used as a substrate for topoisomerase II-mediated relaxation of plectonemes introduced in single molecules using Magnetic Tweezers. The overall rate of relaxation of plectonemes by recombinant human topoisomerase II alpha and *E. coli* gyrase decreased on the stiffer DNA. In addition the binding affinity as well as the ability of *E. coli* gyrase to wrap DNA also decreased. These dynamic measurements of DNA supercoil relaxation by type II topisomerases support the idea that DNA is significantly deformed in the rate-determining step.

DNA elasticity and effects on Type II topoisomerases

By

Qing Shao
B.S., Shanghai Jiao Tong University,
China 2005

Advisor: David Dunlap, Ph.D.

Advisor: Laura Finzi, Ph.D

A dissertation submitted to the Faculty of the
James T. Laney Graduate School Studies of Emory University
in Partial Fulfillment of the Requirements for the Degree of
Doctor of Philosophy
in Physics
2011

Acknowledgement

I owe my deepest gratitude to my advisors, Prof. David Dunlap and Prof. Laura Finzi, for their generous guidance, support and encouragement during the six years of my graduate study. This dissertation would be impossible without their kindly mentorship over my long stay in the Physics Department. It is also because of them, I deeply fall in love with single molecule biophysics.

I also want to express my heartily thanks to my committee members: Dr. Fereydoon Family, Dr. Ivan Rasnik, Dr. Kurt Warncke and Dr. Eric Weeks for their time, thoughtful criticism, encourage and attendance to my annual meetings.

I am grateful to my colleagues, Sachin Goyal, for his dedication to preparation polyamine paper, Kent Lin, for his generous help on EMSA experiments and Finzi group members for assisting me on research.

I would like to also thank my parents, my mother Guanghe Shao and My father Bin Shao for their constant trust on me to encourage me to overcome difficulties during my study.

I am also grateful to my dear friends Hanlin Chen, Jingping Yang and Li Li for their company whenever I need.

I want to thank NSF K-12 program, Emory Science Education Center and Laney Graduate School to offer me financial support to finish my Ph.D. study.

During the six years, I received numerous assistant from members in the Physics Department at Emory. It is impossible to mention all of their names here. The dissertation is dedicated to all of them.

Table of Contents

List of Figures

Chapter 1 Introduction

Chapter 2 Material and Methods

Chapter 3 Effects of polyamines on DNA supercoiling

Chapter 4 Behavior of DAP DNA under tension and torsion

Chapter 5 DNA stiffness affects Type II topoisomerases-DNA interaction and activity

Chapter 1

Introduction

§1.1 Motivation and hypothesis

In cells, the sequence of deoxyribonucleic acid (DNA) with as little as several hundred thousand [1] up to 1-2 hundred billion base pairs [2] is the repository for all the necessary genetic information. In some cases the length of the DNA is as much as a million-fold greater than the available linear dimensions of the cell, and in order to condense this macromolecule in relatively small space, a series of proteins have evolved to package and condense DNA. Among the more famous examples are the histone octamers, which wrap DNA about 1.67 turns around themselves to initiate DNA packaging. Other architectural DNA-binding proteins can bend DNA significantly, such as Integration Host Factor (IHF). In addition to DNA packaging, other important DNA transactions such as transcription and replication are highly regulated by protein-mediated DNA looping, wrapping and bending [3].

For contour lengths greater than a persistence length, which is about 50 nm for natural DNA, the double helix appears to be quite flexible and coil randomly. However, the double helix is so intrinsically rigid that bending it to form arcs shorter than one persistence length requires a lot of energy, around several k_BT. Since DNA stiffness derives from base-pair stacking energy and hydrogen bonding as well as electrostatic interactions, proteins that bend DNA either utilize high positively charged domains to neutralize electrostatic repulsions [4], intercalate in between base pairs, or locally denature DNA to create bends and kinks [5]. Therefore, it is quite natural to hypothesize that transient or more permanent alterations of DNA stiffness might impact the activity of proteins that bind to DNA and produce topological changes.

Tests of this hypothesis may be devised using well established facts. Substantial evidence has demonstrated that polyamines can interact with DNA electrostatically to neutralize the negative charges along the phosphate backbones of DNA and soften the molecule. Indeed one may propose that polyamines facilitate cellular transactions involved DNA bending or

wrapping. Not surprisingly, the levels of natural, positively charged polyamines are often associated with cell growth [6] and rapidly dividing cancer cells [7]. As a prerequisite for this study, a detailed investigation of how polyamines affect DNA stiffness will be presented in the third chapter of this thesis before describing experiments aimed at measuring the rate of topoisomerase activity as a function of DNA stiffness. As a control experiment to exclude the effects of direct interactions between polyamines and protein, it was necessary to perform activity measurements using DNA with intrinsically different stiffness. DNA modified by the substitution of diaminopurine for adenine to increase the number of hydrogen bonds was produced for this "control" experiment and has developed into an interesting object of investigation which is described in the fourth chapter. Finally, experiments described in the fifth chapter reveal how supercoil relaxation catalyzed by two different type II topoisomerases is slower for stiffer with respect to natural DNA. These experiments solidly support the hypothesis that DNA stiffness can affect DNA-protein interactions in which DNA becomes sharply bent.

To summarize, chapter 1 contains some background information about DNA stiffness, polyamines and type II topoisomerase structure and mechanisms. Chapter 2 has the experimental details of the measurements and assays performed, including the Magnetic Tweezers instrumentation, DNA sample preparation, and electrophoretic mobility shift assays. In Chapter 3, the effect of spermine and spermidine on DNA supercoiling is described together with a quantitative interpretation of how the supercoiling properties change as a function of polyamine concentration. Chapter 4 focuses on the description of how the physical properties of DNA, such as stiffness, and response to tension and torsion are affected by the substitution of adenine with diaminopurine (DAP). Finally, in chapter 5, experiments in which DNA stiffness affects its interaction with and the activity of type II topoisomerases are described.

§1.2 DNA primary and secondary structure

§1.2.1 DNA double helical structure is stable

Deoxyribonucleic acid (DNA), a polymer of deoxyribonucleotides, is the repository of genetic information in cells. This genetic information is stored in the sequence of deoxyribonucleotides with four different bases: Adenine(A), Guanine(G), Thymine (T) and Cytosine(G) of which A and G are purines ; C and T are pyrimidines. Bases can interact with each other specifically: A and T form two hydrogen bonds (H bonds), while G and C form three H bonds, respectively when they are anti parallel to each other (Fig. 1.1, top). Therefore, one double stranded DNA (dsDNA) molecule consists of two anti parallel single stranded DNA (ssDNA) linked by the H bonds of the paired bases. In 1953, Watson and Crick determined the secondary structure of DNA to be that of a right handed double helix from previously obtained data [8]. Three features determine the stability and mechanical properties of the DNA double helix [9]. One is the H bonds between base pairs which hold two ssDNA together. These bonds depend on ionic strength [10], temperature [9] , mechanical torque [11], or any other form of energy contribution from the external environment. A second feature is the electrostatics. The negatively charged DNA backbone can interact electrostatically with cations, such as $Mg^{2+,}$ K^{+} and Na^{+} as well as some positively charged biopolymers, such as polyamines [12]. A large number of DNA binding proteins have positive charged surfaces that facilitate interaction with the negative charged DNA backbone [13]. The third feature is constituted by the van der Waals and hydrophobic interactions. The dsDNA base pairs stack together through π, π electronic interaction and hydrophobic forces. This base pair stacking energy contributes significantly to the stability of the DNA double helical structure; therefore, ssDNA, where there is no base stacking, usually assumes the structure of a random coil [9].

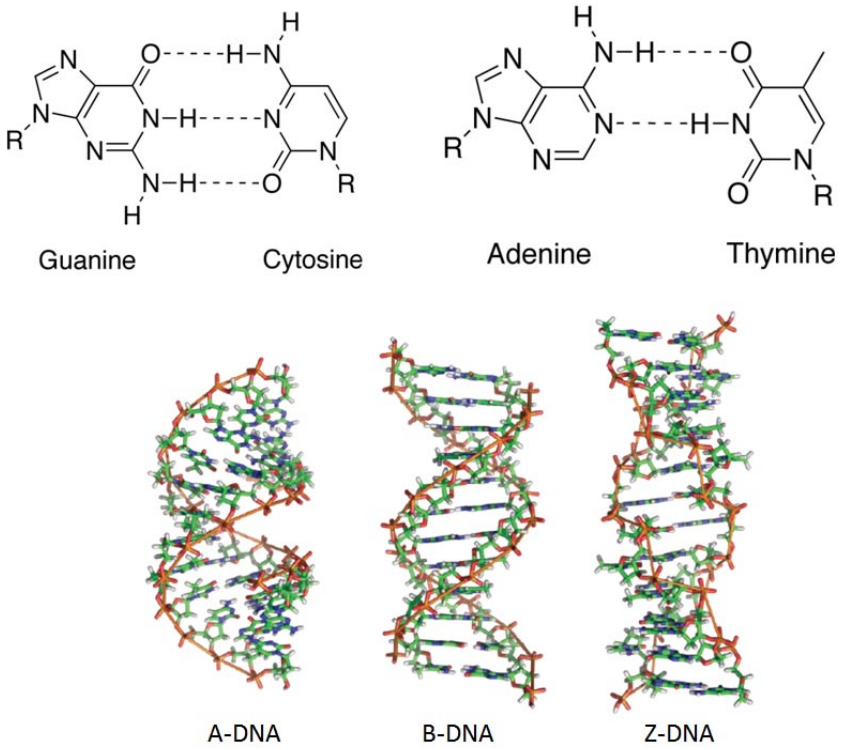

Figure 1.1 GC and AT base pairing and polymorphism of DNA (A, B and Z DNA). By Richard Wheeler.

§1.2.2 Polymorphism of DNA structure: B-DNA, A-DNA and Z-DNA

Double stranded DNA can adopt three major stable conformations: B-, A- and Z -form [14] (Fig. 1.1, bottom). In B DNA, which is most common conformation in aqueous solution, the double helix is right-handed with a helical pitch of 3.4 nm and base pairs separated, in average, by 0.34 nm. Therefore 10 to 10.6 base pairs (bp) are required to complete one helical turn depending on the sequence of DNA. However, in dehydrating conditions DNA adopts the right handed A-form with 2.46 nm helical pitch, 0.23 nm base pairs separation and 11 bp per helical turn. In contrast, Z-DNA is a left-handed dsDNA with 4.6 nm helical pitch, 0.38 nm base pairs separation and 12 bp in one helical turns. The B- to Z- form transition is often

observed in DNA with alternating pyrimidine-purine (G:C –C:G) sequences. The transition is triggered by high concentration of salts [15] or addition of alcohol [16] through rotation of the base pairs. Although, B, A and Z-form DNA each have distinctive structural characteristics, they could coexist in long DNA molecules where short regions of A and/or Z form, due to sequence differences or distortion by DNA binding proteins, are interdispersed in long stretches of B-DNA, [17, 18].

§1.3 DNA behavior under tension and torsion

§1.3.1 Stretching and twisting single DNA molecule

In cells, DNA is always involved in a great number of cellular processes, motor proteins can apply tension or torsion on DNA molecules when they bind and process DNA. For example, *E.coli* RNA polymerase can apply forces up to 20 pN during transcription [19], DNA helicases must generate forces between 10 – 15 pN to unzip dsDNA [20] and bacteriophage Φ29 packing machine can pack DNA against forces up to 57 pN [21]. Therefore, understanding DNA behavior under tension and torsion is very important for the understanding of DNA transactions. Single molecule manipulation techniques emerged in the early 1990 started a new era of investigation of the effect of tension and torsion on DNA. These new techniques include: Optical Tweezers [22], Magnetic Tweezers [23], Atomic Force Microscopy and Spectroscopy [24]. Almost all of these techniques require immobilization of single DNA molecules on a surface. Specifically, the DNA molecule is anchored on the immobilized surface on one end and to a force sensor, polystyrene bead, magnetic beads or micro cantilevers, at the other end. By monitoring the position or fluctuation of the force sensor, the behavior of DNA under tension or torsion can be revealed. The dependence of the DNA end-to-end distance (DNA extension) on external forces below

60 pN is shown in figure 1.2. This force vs. extension curve can be fitted using the Worm-like-Chain model [25] (Eq. 1.1). z is the extension of DNA (end to end distance), F is the tension applied on single DNA molecule. One of the fitting parameters "P" is called persistence length, and represents the stiffness of the DNA molecule: the longer the persistence length, the stiffer the DNA molecule. L is the contour length of DNA.

$$F = \frac{k_B T}{P}\left[\frac{1}{4(1-z/L)^2} - \frac{1}{4} + \frac{z}{L}\right] \qquad \textbf{[Eq.1.1]}$$

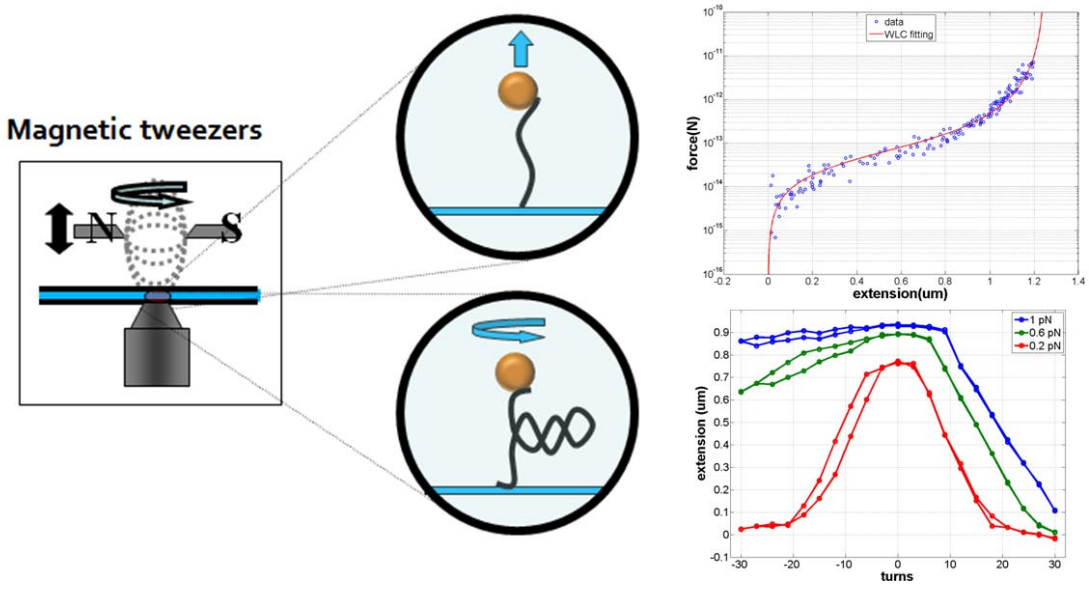

Figure 1.2 Magnetic Tweezers setup and DNA behavior under tension and torsion. Left. Schematic experimental set up. Top Right. Force vs. DNA extension data (open circle) and WLC fitting of the data (red line); Bottom right. DNA extension vs. magnet turns curves (hat curves) at different forces with different color codes. Data are collected in our lab

The persistence length of normal B-DNA is about 50 nm in physiological conditions [26]. Torsion can be applied to single DNA molecules by rotating the sensor: quartz cylinders for

Optical Tweezers [27] and paramagnetic beads for Magnetic Tweezers [23] at different forces as shown in figure 1.2.

At low force, less than 1 pN, positive and negative supercoils form when DNA is wound or unwound, respectively. The formation of DNA supercoils results a decrease of the DNA extension. However, since B-form DNA is a right handed molecule, when the force is high enough, the unwound DNA does not buckle, but is thought to denature [11]. In this situation, the extension remains unchanged, because no DNA fragment is absorbed to the plectonemic form [23]. The behaviors of wound DNA and shape of plectomes that form are studied theoretically using elastic rod model [28-30]. Therefore, by investigating DNA extension under tension and torsion, mechanical properties, such as persistence length (bending rigidity) [25] and torsional persistence length (torsional rigidity) of DNA [31] may be characterized in different buffer conditions.

§1.3.2 DNA phase transition under extreme tension and torsion

Very high force, over 60 pN, and torque, over 10 k_BT, can trigger DNA phase transitions. "DNA phase diagrams"(Fig. 1.3) obtained recently by single-molecule experiments have revealed the existence of different helical forms of DNA stabilized by external force and torques [32]. The number of turns has been normalized as $\sigma = (Lk - Lk_0)/Lk_0 = n/Lk_0$, where Lk_0 is called linking number which represents the number of right-handed helical turns in the torsionally-relaxed state of B-form dsDNA, and n is the number of rotations added to the DNA. Lk represents linking number of DNA under torsion. Lk can be equated to the twist and writhe, where writhe is the number of supercoils and twist is the number of helical turns.

The B phase represents B-DNA which is stable at forces ranging from 0 to 60 pN and positive torque less than about 9 k_BT. Once the force is increased to about 65 pN, DNA

displays a transition to an extended form which is 70% longer than normal B-form [33]. This form is called over stretched DNA and “S” is the letter represents this form in the phase diagram. However, if force and torque increase simultaneously, DNA will adapt an extended form, the Pauling DNA, “P” in the diagram, characterized by exposed bases [34]. “Sc-P” is the supercoiling form of Pauling DNA which is postulated to occur at torque larger than 10 k_BT. The most mysterious phase happens when DNA is under extreme twist. In the phase diagram, “L” indicates DNA with an average left handed twist [32], L-DNA, not necessarily Z-DNA. Most recent twisting experiments at high force in Michelle Wang’s group indicate this DNA structure to be a left-handed double helix with no pairing. However, the transition from B-DNA to L- DNA shows sequence dependence and hysteresis back from L-DNA to B –DNA. Whether the transition involves base pair melting or local right handed to left handed conversion is still unclear.

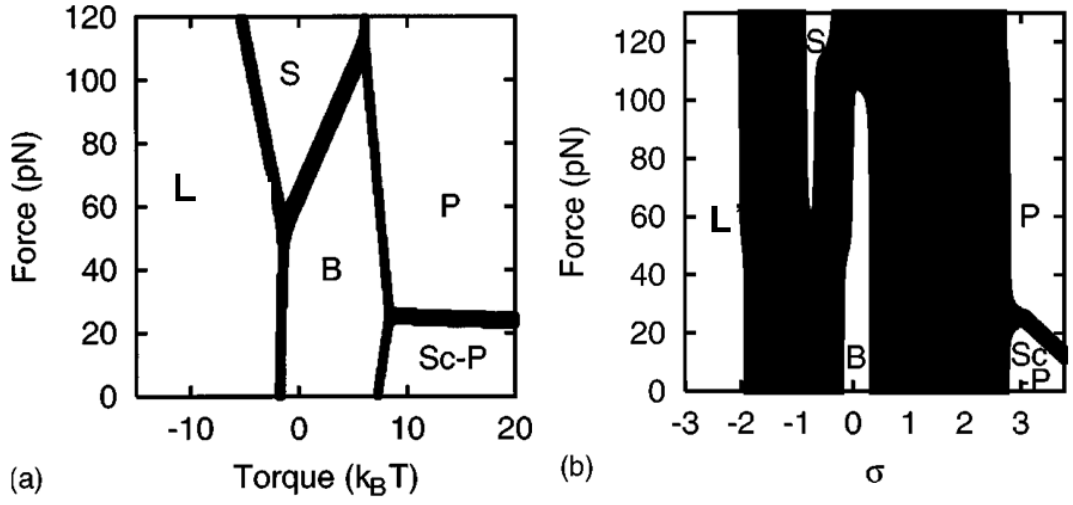

Figure 1.3 Force-torque (a) and force-σ (b) phase diagram of DNA. Adjacent phases coexist inside the black boundaries, each phase is pure within a given area of the diagram. Reproduced from [32].

§1.4 Why is DNA a stiff molecule?

§1.4.1 Definition of DNA stiffness and experimental methods to study it

Among the natural polymers, DNA is one of the stiffest ones. The bending rigidity of dsDNA exceeds that of amino acid polymers by approximately 20 fold [35]. The stiffness of the DNA is a potential obstacle for proteins which bend, twist and loop DNA. Therefore, understanding the physical properties (stiffness) of DNA is very important to study the protein-DNA interactions which lead to significant DNA conformational changes important in the regulation of cellular processes. DNA stiffness can be described using two mechanical parameters: bending and torsional persistence length representing the flexural and torsional rigidity of the DNA molecule, respectively. In the absence of applied force or torque, DNA molecules that are shorter or equal to the persistence length, behave like rigid rods, while DNA fragments much longer than the persistence length, behave like random coils. Various single DNA manipulation techniques can be used to measure the bending and torsional persistence length of DNA. For example, Atomic Force Microscopy can be used to image the contour of DNA molecules. The persistence length can be derived by using the worm-like-chain (WLC) model to fit the end to end distance of the DNA molecule as measured from the AFM image [36]. Similarly, by stretching single DNA molecules with Magnetic Tweezers [23] or Optical Tweezers [37], DNA persistence length can be obtained by using the WLC model to fit the force vs. extension data . The bending persistence length of DNA measured by these methods is about 50 nm on physiological condition, which agrees well with that from bulk experiments [38]. In addition, one may derive the DNA torsional persistence length using Rod Like Chain model to fit the curve of DNA extension vs. number of turns [39], or may calculate it from experimentally measured [27] or estimated [31] torque values on single

DNA molecule. The torsional persistence length is between 75 nm and 100 nm depending on force and ionic strength in the solution.

§1.4.2 The origins of DNA stiffness

Although stiffness is a very important physical property of DNA, its origin is still under investigation. As mentioned above, three factors contribute to the DNA stability, electrostatic interactions of negative charged DNA back bone, H bonds within the base pairings and base pair stacking interactions. These factors are thought to be the most important contributors to the DNA stiffness [40] as shown in figure 1.4. Specifically, negatively charged phosphate groups along the DNA backbone produce a repulsive force on DNA, this force results in an increased separation between base-pairs [41]. The neutralization of those negative charges by counter ions either in solution or on surface increases DNA flexibility by decreasing this self repulsive force [36, 42]. Base-pair stacking interactions which tend to contract the double helix due to electrons interaction also contribute to the DNA stiffness significantly. Transient electric birefringence (TBE) shows that single-stranded poly-pyrimidine base pairing with free purine bases exhibiting duplex character was much more flexible than the equivalent full dsDNA [43]. H bonding is essential to maintain helical form of double strand DNA and bridging two single strands. Experimental data show that, the persistence length of ssDNA without base-pairing is around 3 nm [44], which is much smaller than that of dsDNA. These contributions are also supported by the evidence that DNA persistence length is influenced by the sequence-dependent difference in base pair stacking forces and number of H bonds [45]. Considering the relative motion of base-pairs upon external stretching or twisting of DNA molecule, both base pair stacking interactions and electrostatic repulsion affected these motions. Therefore, studying the flexural and torsional rigidity of DNA under different

stacking and electrostatic conditions may yield insight on the origins of DNA stiffness. The approach to alter the electrostatic interactions by introducing monovalent and multivalent cations has already been followed extensively as mentioned before. However, another group of counter ions: positively charged biopolymers such polyamines which play very important role in cellular process also need to be considered. The investigation on how those polymers affects DNA behavior under tension and torsion is crucial to understand the effects on how electrostatic interaction affects DNA stiffness in the cellular environment where they are expressed at different levels during different times.

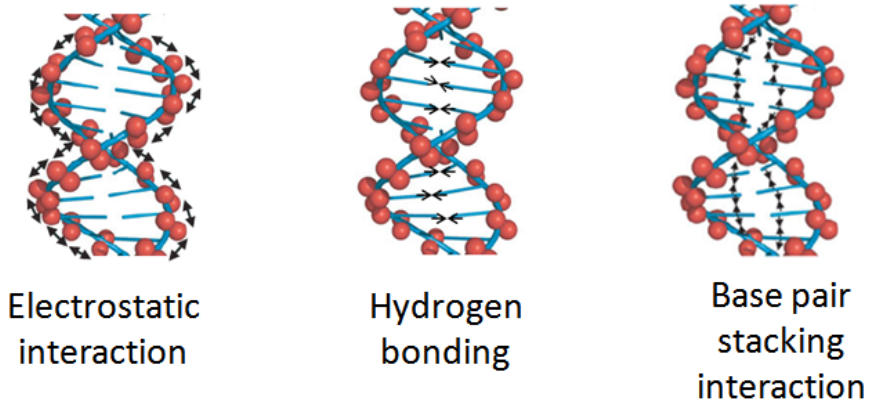

Figure 1.4 Schematic illustrations of the origins of DNA stiffness. [40]

While, one of the methods to vary base pair stacking energy is base substitution. Substituting adenine with 2,6 diaminopurine (DAP) in dsDNA results in three H bonds between DAP and T instead of the two in AT base pairs, and it contributes one lonely electron pair on nitrogen atom from the extra amino group to π,π interactions with the adjacent base pair [45]. AFM data shows that, DAP substitution increases the persistence length by 20% [45]. According to NMR studies DAP-substituted DNA remains in B-form [46]. Therefore, DAP-substituted

DNA lends itself to be an optimal model to study the effect of increasing base pair stacking on DNA stiffness, and to see how DNA stiffness affects protein interaction and activity.

§1.4.3 DNA stiffness affects DNA-protein interactions

Flexibility measurements using AFM imaging shows that DNA persistence length is influenced by the DNA sequence: AT rich DNA is characterized by about 10% shorter persistence length [45]. Nucleosome reconstitution assays show that histone octamers have higher affinity for AT rich DNA fragments [45], which supports the idea that these sequences are more flexible than others. Besides, since AT base pairs are less stable than GC base pairs, kinks, which might involve base pair breathing, are most probable in AT rich regions. This is supported by the data showing that the binding of IHF, which bends DNA by 160-180 degrees, is affected significantly by substitution A to 2,6 diaminopurine (which can form three H bonds with T) at kinking sites [47].

§1.5 Natural polyamines (spermine and spermidine)

Polyamines are organic compounds having more than one amino group (NH2). They are synthesized in living cells via highly regulated pathways and are known to regulate cell growth, gene transcription and activation of DNA synthesis [6]. High levels of some polyamines are often associated with cancerous cells [7]. Furthermore, increased polyamine levels are diagnostic markers of drug resistance in treatment of cancer patients [48]. How polyamines participate in cellular metabolism to influence growth or cancerous behavior is not entirely understood. Perhaps, a stepping stone for this research quest is to investigate how polyamines influence the physiologically relevant structural changes in deoxyribonucleic acid

(DNA). To elucidate this connection, we begin by discussing the physiologically relevant structural changes in DNA, then look at how much is already known about DNA-polyamine interactions, and finally describe how and what we may contribute further to this knowledge.

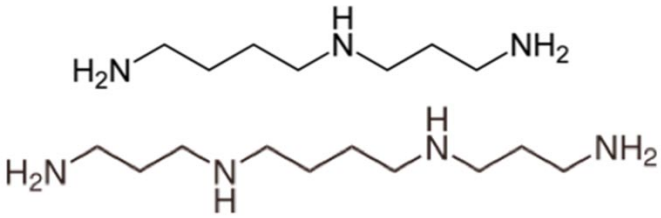

Figure 1.5 Schematic structure of the two polyamines spermidine (top) and spermine (bottom). They are long cations due to the positive amino group (NH2) in solution of physiological condition.

§1.5.1 DNA supercoiling regulates DNA topology, DNA replication and transcription

Inside living cells, DNA is always organized in high-order topological structures. One of the physiologically relevant tertiary structures is an intertwined structure called “plectonemic" DNA. In plectonemic DNA the double helical axis is folded into a superhelix. Plectonemes are essential to keep DNA condensed in prokaryotic cells. Furthermore, plectonemic supercoiling not only regulates the topological features, writhe and twist, of DNA, but also plays a crucial role in the regulation of DNA transcription and replication [49]. Bacterial plasmids are always found to be negatively supercoiled [50]. Negative supercoiling often causes local denaturing of DNA in promoter regions and at the origin of replication to

facilitate initiation of DNA transcription and replication, since both processes require polymerase binding on a single strand of DNA [49]. By contrast, positive supercoiling interferes with mRNA synthesis by slowing down the processivity of RNA polymerase [51]. Thus, to regulate cellular functions and growth, there must be a mechanism to regulate DNA supercoiling. Topoisomerases constitute a family of enzymes that provide the mechanism to regulate DNA supercoiling. For example, in a prokaryotic cell, while topoisomerase I relaxes negative supercoils by binding a locally denatured DNA segment, gyrase introduces negative and relaxes positively supercoils [49], while in eukaryotes cell, topoisomerase II can relax either positive or negative supercoilings by strand passage mechanism. Therefore, the DNA supercoiling is systematically regulated by several enzymes to ensure an optimal performance of the cellular functions.

§1.5.2 Polyamines can interact with DNA electrostatically

Understanding how polyamines affect DNA supercoiling is therefore very important. Some experiments suggest that polyamines facilitate the condensation of DNA [52], protect it from radiation and oxidation [53, 54] and stabilize its right-handed, double helical B-form structure [55]. One may expect polyamines, which have positively charged amino groups distributed along their lengths, to interact electrostatically with the negatively charged phosphate backbones of DNA. In fact, recent infrared data suggest that some polyamines bind to the major and minor grooves of DNA to interact with the bases [12], wherein it is also noted that the preference of binding modes depends on the sizes of polyamines. Spermidine, which has three amino groups, and spermine, which has four amino groups (Fig. 1.5) are two most commonly occurring polyamines in mammals [56], which bind to the major and minor grooves of DNA [12, 57]. However, little is known about how the two polyamines affect DNA supercoiling.

§1.5.3 Spermine and Spermidine affect transcription modifying the level of DNA supercoiling

Researchers have found that the two polyamines, spermine and spermidine can increase the positive supercoils formed during transcription, In particular, it was found that the presence of polyamimes can maintain the transcription rate respect high level of positive supercoiling [58]. This effect is believed to result from the fact that polyamine could change the physical property of DNA supercoils [58]. Moreover, polyamines have been reported to interfere with the relaxation of negative supercoils by Topoisomerase I , and this effect has been attributed to the stabilization of the DNA double helix by polyamines [58]. Increase in positive supercoiling during transcription and inhibition of Topoisomerase I, are both observed when either spermine is present in submillimolar or spermidine is present in millimolar concentration [58], which are the physiological concentrations of the two polyamines [56]. Although qualitative explanations have been proposed for these effects [58], the details on how polyamine quantitatively regulate DNA supercoils haven't been investigated, although systematic regulation of the concentration of the polyamines [6] has to be one of the most important mechanisms for a cell to regulate the supercoling related enzyme activities and cellular processes.

§1.5.4 Single molecule studies of DNA condensation by polyamines

Previous single-molecule experiments have taken advantage of Magnetic Tweezers to analyze the role of the two polyamines as DNA condensing agents by investigating the dependence of condensation on tension [59] and twist [60] at various polyamine concentrations. More specifically, these experiments have focused on looking at the condensation forces, which were found to be up to 4pN for spermine and 3pN for spermidine. The condensation forces depend on the polyamine concentration and free energies, which

were reported as -0.33 k_BT/bp for spermine and -0.2 k_BT/bp for spermidine. The data was measured by relaxing DNA from high tension (lager than 10 pN) at up to 80 twisting turns.

§1.6 Type II DNA topoismoerases

Type II topoisomerase is an essential cellular ATP dependent enzyme that segregates newly replicated chromosomes during cell division and maintains the supercoiled state of DNA [61]. Since studies show that some type II Topoisomerases in eukaryotic cancer cells are expressed at high levels in order to maintain the high division rate, inhibiting the function of Type II topoisomerases can prevent chromosome segregation in cancer cell, therefore, Type II topisomerases became one target of treatment of tumor cells [62].

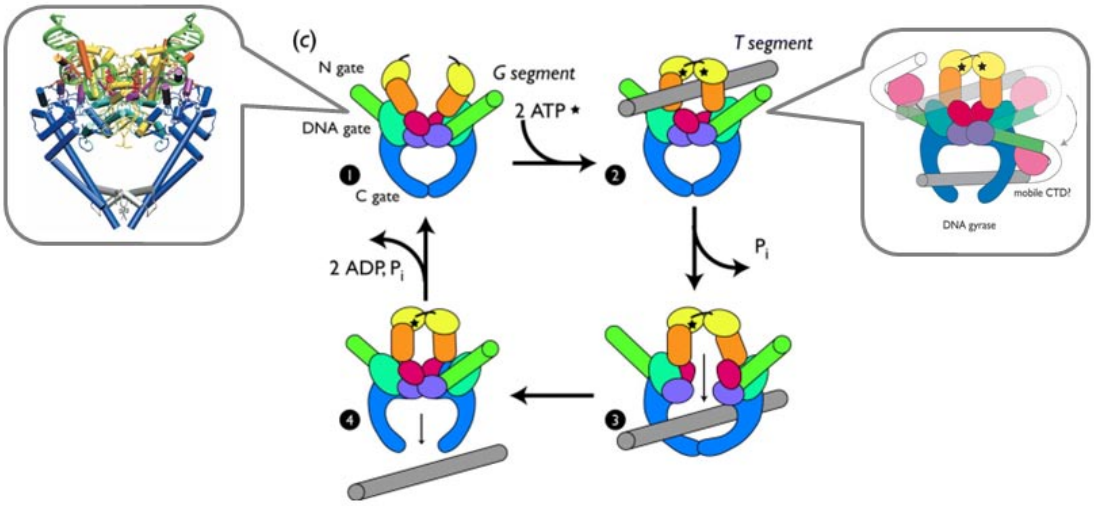

Figure 1.5 Type II topoisomerases structure and mechanism. Green and grey rods represent different DNA segments. Crystallized structure of Type II topoisomerase DNA complex (left) [63]; DNA wrapping around the C terminal domain of gyrase (right) [62]

§1.6.1 Structure and function of Type II topoismoerases

Type II topoisomerases are homodimers in their active form. The two monomers in the enzyme adopt a structure that forms three gates, the N-terminal gate, DNA gate and C-terminal gate and two chambers. The two chambers are two cavities separated by the three gates [64] . The N-terminal gate consists of two elements: an ATPase region and an adjacent region which connect to the DNA gate of the enzyme. The DNA gate is the catalytic center of the enzyme: A divalent metal-bind topoisomerase-primase (TOPRIM) domain, a winged-helix domain (WHD) where the catalytic tyrosine is located and a tower structure composes the DNA gate [65]. The C-terminal gate is formed by two coiled-coils extended from the α/β fold adjacent to the WHD [65]. Type II topoisomerases employ a strand passage mechanism to resolve DNA entangles. During the catalytic cycle, the DNA gate first binds one segment of the supercoiled double helix, called gate segment, waiting for another DNA segment, the transfer segment, to enter the N-terminal gate [66]. The binding of two ATP molecules to the ATPases leads to the closure of the N-terminal gate around the transfer segment and triggers the enzymatic reaction [66]. The catalytic tyrosines manage to form covalent bonds with 5'-phophoryl groups located on the opposite single stands separated by four base pairs. Those two covalent bonds between DNA and enzyme cause DNA nicks in each single strand. After one ATP molecule is hydrolyzed, the DNA gate opens the cleaved DNA by moving the TOPRIM and WHD domains from each monomer away from each other [65]. The open DNA gate offers the path for the transfer of the DNA segment into the lower chamber. The gate segment of DNA is religated after strand passage. This conformational change triggers the C-terminal gate to open and release the transfer segment from the lower chamber [18].

§1.6.2 Type II topopisomerases can bend DNA during the enzymatic cycle

Crystallographic data shows that the type II topoisomerases can bend gate segment significantly to accommodate the active conformation of the enzyme [18, 67]. The bend is achieved by two sharp 75 degree bending fulfilled by intercalating a β hairpin from WHD into bound DNA gate segment [18]. Although being cataloged as a nonspecific enzyme, kinetic and thermodynamic data show that type II topoisomerases selects DNA cleavage sites based on reactivity [68]. This finding suggests that DNA bending may be the reason for these preferred sites of cleavage. *E. coli* gyrase, one of the type II topoisomerase can wrap about 100 bp DNA around its C-terminal domain (CTD) up to 180 degrees to facilitate introducing negative supercoiling and relaxing positive loops of supercoiling [4]. The dramatic DNA conformational changes observed during the enzymatic cycle of type II topoisomerases indicates that DNA stiffness may affect the rate limiting step of the enzymes. Besides type II topoisomerases, there is a large number of proteins which bend or wrap DNA to fulfill their tasks, including regulators of DNA replication and transcription. The integration host factor (IHF) and the heat unstable (HU) protein can bend DNA significantly [5, 69], and their bindings may be affected by the DNA stiffness. DNA wrapping around histones chromatin also depends on DNA stiffness [45]. Similar to DNA bending proteins IHF, electron micrographs reveal that most Type II topoisomerases bind at the highly curved apices of supercoiled plasmid [70]. In addition, Systematic Evolution of ligands by Exponential Enrichment (SELEX) and kinetic analyses associating with tens of base pairs short DNA fragment indicate that AT rich regions are preferentially cleaved by type II topoisomerases [71] and sequence dependent cleavage specificity happens after DNA binding [68]. These observations indicate that sequence-specific DNA bending is most likely to occur to facilitate the cleaving of DNA to accommodate significant conformational change of enzyme in the enzymatic cycle.

§1.7 Experimental techniques

§1.7.1 Principle and Development of Magnetic Tweezers

Manipulation of single DNA molecule using a magnet was first introduced by Smith and Finzi in 1992 to pull on DNA [72]. Several years later, Croquette and Bensimon established the prototype of Magnetic Tweezers (MT) widely used today to both pull and rotate DNA [23]. The basic setup of MT includes a pair of permanent magnets placed on a stage which controls the translational and rotational movement of the magnets. The magnetic field created in space can induce the magnetic moment of the paramagnetic bead attached to biomacromolecule. The force applied on the paramagnetic bead is proportional to the gradient of magnetic field *B* and the induced magnetic moment *m* as follows: $F = \frac{1}{2}\vec{\nabla}(\vec{m} \bullet \vec{B})$. The relation between the force and distance from magnet to the sample highly depends on the geometry of the magnetic field. In our case, the gradient of the magnetic field increases with decreasing of distance between beads and magnets. Therefore, the magnitude of the force can be correlated with the magnet position, which means users can achieve difference force values by changing the vertical position of the magnets. In addition to the distance, the size and material property of the beads also contribute to the magnitude of the force. Because the magnetic moment of the super paramagnetic beads, expressed as $\vec{m} = V_b \chi \vec{B} / \mu_0$, highly depends on their susceptibility χ and volume V_b. The force felt by each bead will be different because of the slightly differences in size and magnetite content [73]. Therefore, it is not practical to calculate the force by measuring the strength of the magnetic field in space. Instead, the standard method to determine force value is to apply the equipartition theorem and pendulum model (DNA tethered bead) to individual DNA tethered bead. The equation to calculate the force is: $F = k_B T l / \delta x^2$, where $k_B T$ is Boltzmann constant

times temperature, l is the extension of DNA and δx^2 is the mean square of the bead's fluctuation in the x direction which can be measured experimentally by tracking the center of DNA tethered bead [23]. In addition, since the induced magnetic moment in the beads must align with the direction or the lines of the magnetic field, the rotation of the magnetic field will result in the rotation of the bead in order to maintain the alignment of magnetic moment. Therefore, as a consequence of the geometry of MT (Fig. 1.2), the bead will rotate with the rotation of the magnets, so the torque applied to the bead will transmit to the attached DNA. However, because of the rotational symmetry of spherical beads, it is impossible to detect its angular fluctuation; therefore using MT to experimentally determine the value of the torque is still a challenge. Recent development in theory and instrumentation enables the calculation of torque from extension vs. magnet rotation data [31] [74] or from the detection of angular fluctuation by attaching an angular sensor to the paramagnetic bead [75]

§1.7.2 Principle and application of EMSA

Electrophoretic Mobility Shift Assay (EMSA) is a widely used technique to study DNA – protein interaction. This mobility assay is based on the electrophoretic separation of protein bound DNA and free DNA on a polyacrylamide gel. The migration speed of a molecule moving in the gel is determined by its size and charge, so the large protein-DNA complex exhibits low mobility compared to free DNA, and the more protein binds to DNA, the lower mobility the complex has [76]; therefore, EMSA can be also used to determine not only the specificity of DNA binding proteins to certain DNA sequences, but also the number of binding sites on a DNA molecule. EMSA may also be used to find the amount of protein necessary to saturate a given piece of DNA in order to quantitatively determine the dissociation constant of an enzyme from DNA [77].

In EMSA, DNA is always labeled either with isotope ^{32}P or fluorescent dyes to be visualized in the gel [78, 79]. The labeling plays a role as a probe as well as signal amplification tool, either increasing exposure time for ^{32}P or increase the intensity of excitation light for florescence labeling can enhance the intensity of the signal from DNA bands on the gel. Therefore, EMSA only requires a very small amount of labeled DNA as well as proteins for the visualization of the bands. Practically, a small amount of free DNA without protein runs in one lane as the control to ensure the band shift isn't caused by effects other than protein binding, the same amount of DNA in the presence of different amounts of protein will run in various other lanes. If the protein binds to DNA, the protein-DNA complex will run more slowly than free DNA and the DNA position will be shifted. In each lane, the ratio between the intensity of the bands of free DNA to protein-DNA depends on the protein concentration. The intensity of the bands can be quantified using image analysis software.

Chapter 2

Material and Methods

§2.1 Magnetic Tweezers instrumentation

§2.1.1 Hardware of a Magnetic Tweezers Microscope

The Magnetic Tweezers microscope used in my project was composed by the following parts in Figure 2.1: illumination unit, magnet control unit, sample stage, objective control unit and image acquisition unit (Figure MT). All these components were aligned along a vertical optical rail in sequence, and the optical rail was supported on a vibration damped optical table.

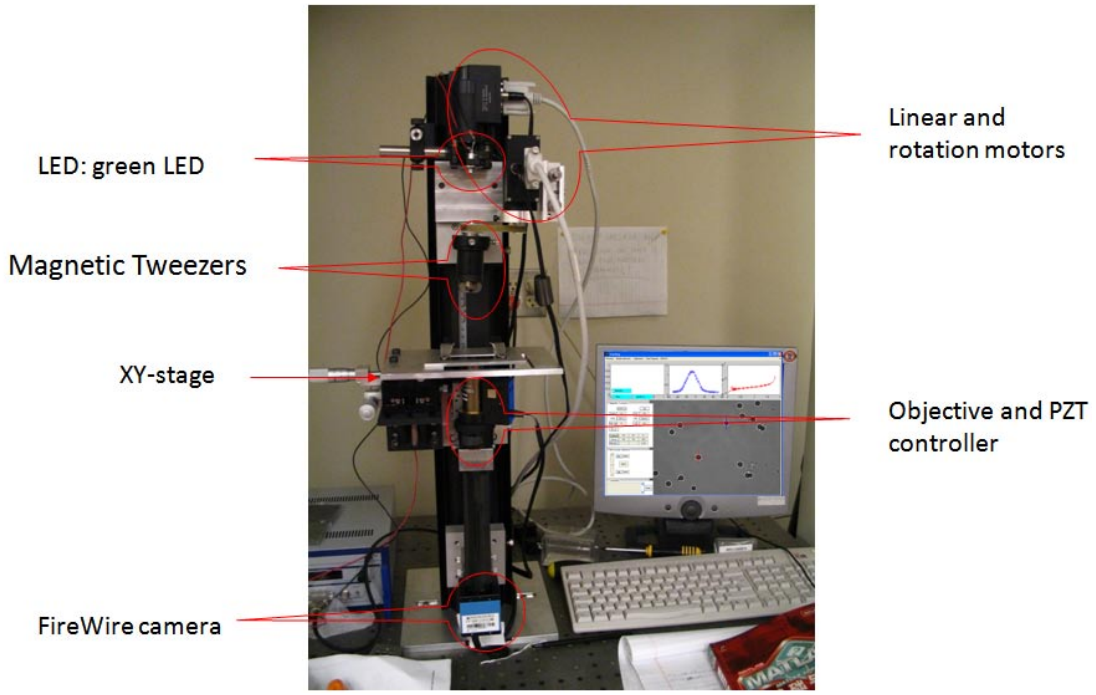

Figure 2.1 Magnetic Tweezers Microscope instrumentation

We used a green LED (LED supply l1-0-G5TH15-1) as the light source. The circuit to power the green LED was consisted of one 12.6 V standard DC power supply, a 270 Ω resistor to set the current around 20 mA (the working current for the LED). This green LED was inserted in

a hollow aluminum adapter and secured by a set screw. A small convex lens was placed underneath the green LED within the adapter to gather the diverging light into a parallel beam directed to the sample. This assembly was placed inside a kinematic mirror mount (Thorlabs), and then mounted on the vertical rail.

The magnet positioning assembly included one translational stage (M-126 PD2 from PI), one rotary motor (C-150 PD from PI) and a pair of N50 grade neodymium magnets with soft iron pole pieces. The rotary stage and magnets were mounted on the translational stage to such that they could travel vertically. The rotary stage controls the rotation of the magnet tweezers through belt-driven, 2:1 reductive gearing. The magnets were composed by four permanent, rectangular block magnets in the middle held in two soft iron semi-cylinders, and an iron yoke placed between lower parts of the semicylinders with the gap smaller than 1 mm for the light to go through from the top (figure 2.2).

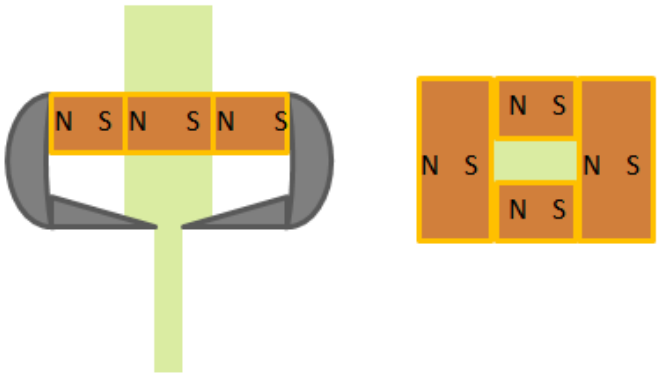

Figure 2.2 Schematic structure of the magnets. Grey color indicates the material is soft iron, the brown color blocks are the four permanent magnets. Left is the side view and right is the top view of the arrangement of magnets. Light green represents the green illumination light

The sample stage was fashioned from an aluminum plate mounted on two manually operated micropositioning stages. The sample stage was designed to accommodate flow chambers made from slides, cover slips, and a commercially available thermostatic cell.

The objective control unit consisted of one 100x Nikon oil immerse objective mounted on a piezoelectric focusing system (P-721.CDQ, PI) attached to a vertical translation stage (Newport). The micrometer driven controlled stage was used to coarsely position the objective throughout a 10 mm range, while the piezo under the control of the E665.CR, controller (PI) provided submicron precision in objective positioning across a 100 micron range.

The image acquisition unit began with a convex, relay lens to focus the parallel light from objective on a CCD camera. The CCD camera was connected to computer through the firewire (IEEE 1394) port. The images arriving from the camera were analyzed by custom software routines in real time.

§2.1.2 Software of Magnetic Tweezers Microscope: controller interfaces

The software controlling the Magnetic Tweezers microscope and image processing was developed by Dr. Carlo Manzo, former postdoctoral fellow in Finzi Lab. The software was written in Matlab, and the graphical user interface was designed for image visualization and instrument control as well as real time data processing as shown in figure 2.3

The parts controlled by the software included the translational stage and rotary motor, the piezoelectric focusing system, and the CCD camera. The translational and rotary stages were connected via cables to serial ports on C843 controller board (PI) inserted into a slot on the motherboard of the computer. To establish control, a dynamically linked library (DLL) file

from PI (C843_GCS.DLL) was loaded into Matlab to provide control of the position, speed and direction of the translational and rotary stages. Similarly, another DLL file was loaded in Matlab to control the movement of the piezo focusing system via the controller (close loop mode) connected through the series port on the motherboard of the computer. The 'dcam' driver developed by Carnegie Mellon University was installed to control the firewire CCD camera using Matlab.

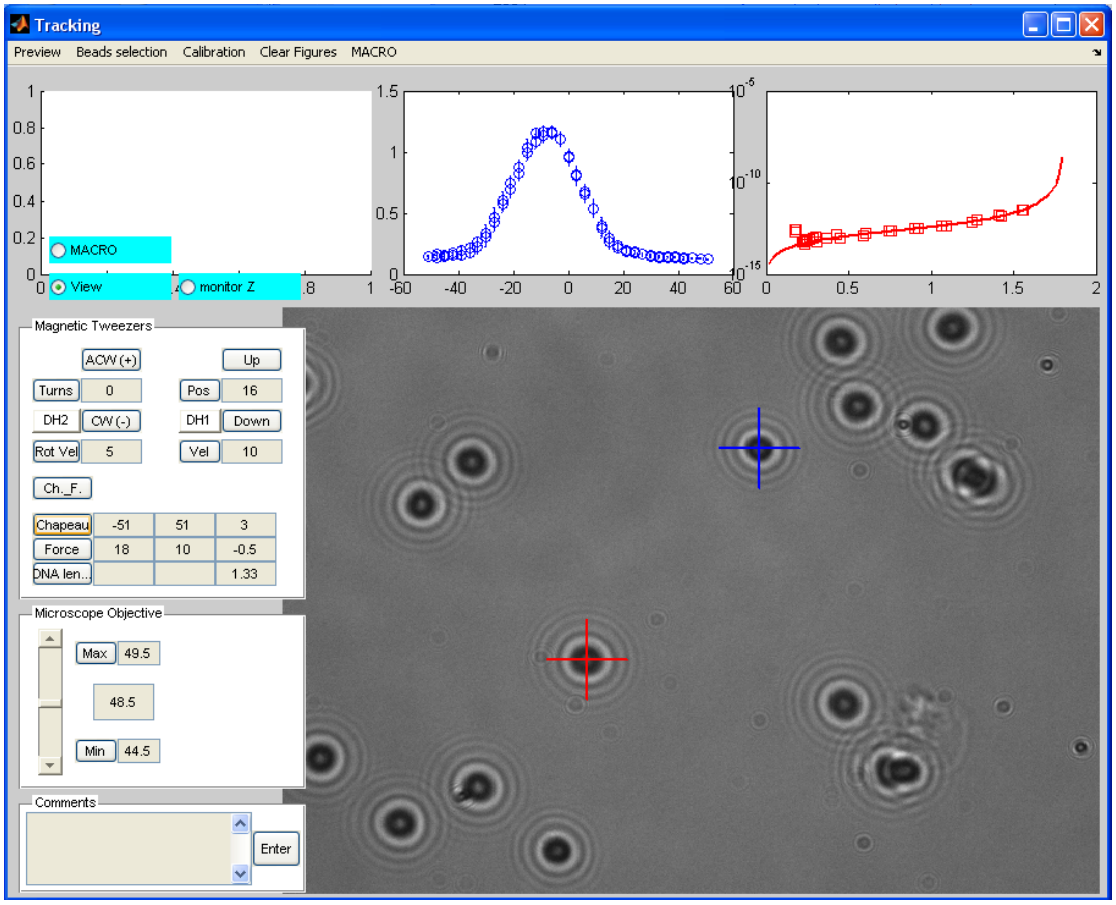

Figure 2.3 Graphic interface of the Magnetic Tweezers Microscope software. (provided by Yue Ding)

Images were visualized using the commands from image acquisition tool box in Matlab. The maximum frame rate of the CCD camera is 60 frames/s. However, since the bead tracking involved computing correlation and convolution, data could only be obtained at about 20 frames/s. The images were 640×480 pixels in size with 0.56 micron per pixel.

Real-time image processing was used to track the positions of the bead in video streams. By tracking beads three dimensionally, I monitored the extension of DNA in order to calculate the force exerted on the bead by the magnets at various positions. The XY positions were determined by convolving consecutive images. The z position was determined by creating a series of progressively more over focused images using the piezoelectric objective positioner and then choosing the most similar diffraction pattern (rings) of the DNA-tethered bead and the bead stuck on the glass surface. The tracking uncertainty of x, y, z coordinates is about 20 nm in this system.

§2.1.3 User manual of the software of Magnetic Tweezers Microscope

The software interface of the Magnetic Tweezers is shown in figure 2.3. There are three main panels in this interface: the image view panel (in the middle of the window), the magnet and objective control panel (along the left side of the window), and the data visualization panel (along the top of the window). There is also a menu list including sub-menus called preview, beads selection, calibration and etc.

The image view panel displays the live image from the CCD in real time to allow users to adjust the focus and select and monitor target beads. Since the instrument utilizes bright field illumination and monochromatic CCD camera, the images of the beads display diffraction rings patterns in a grey scale.

In the magnet and objective control panel, there is a sub-panel called “Magnetic Tweezers”, in which the user can specify the magnet position in the field next to the ‘Pos’ button and send command to the translational stage to move magnet up or down in a range from 1-19 mm, with 1 mm is the farthest separation from the sample stage. The translational stage can reach 20 mm; however, at 19 mm, the magnets almost touch the upper surface of the chamber. Likewise, the stage can reach 0 mm, however, this will trigger self locking mechanism of the translational stage. The velocity of translational stage can be specified in the field labeled ‘Vel’. Similarly, the number of turns and rotation velocity can be set using fields labeled ‘turns’ and ‘Rot Vel’ respectively. The direction of rotation is determined by the sign of the ‘turns’ entries, positive values produce clockwise rotation and negative values counterclockwise.

There are three functions in the lower part of this subpanel to automate data collection over a range of tension or rotation values. The “chapeau” function records the extension of the DNA tether vs. twist applied using the magnets. In the three fields next to the “chapeau” button, users input the minimum and maximum values and the increment of the independent twist variable. Once the chapeau button is clicked, the software will automatically measure the DNA extension at each twist value proceeding from the minimum to the maximum value with specified increments. The DNA extension vs. turns data are plotted in the central sub-panel in the data plotting panel. Similarly, another function called “force” automatically measures tension stepping through different magnet positions from a minimum to a maximum value in specified increments. The force vs. DNA extension data is plotted in the right sub-panel of the data plotting panel. The third function is called “Ch._F.” This function automatically records extension vs. turns data at a series of different tensions (magnet positions), the input parameters are read from the fields next to “chapeau” and “force” buttons.

The sub-panel “microscope objective” is a user interface to control the piezo which positions the objective to adjust the focus of the image. Users can specify the objective position by inserting a value in the middle field or use the scroll bar to set the position. The fields next to “Max” and “Min” are used to specify maximum and minimum values of the objective position during the collection of images used in tracking beads along the *z* axis (optical axis). Just below is a ”Comment” sub-panel to allow the user to take notes of experiments and save the notes in a text file.

The left sub-panel in the data plotting panel is used to plot the *z* position of the reference beads (red) and DNA tethered bead (blue) in order to monitor any changes in the extension of the DNA tether during an experiment. Recordings of the *x*, *y*, and *z* coordinates of a reference bead and a DNA-tethered bead in a text file can be initiated by deactivating the “view” button underneath the sub-panel. Alternatively a user can choose to plot the data in the sub-panel in real time by selecting the “monitor Z” button.

At the top of the frame there is a menu bar. The leftmost menu is “preview”. Clicking the “preview” button, opens a drop-down menu with “start” and “stop” which start and stop image video streaming from the CCD, and “close” which terminates the Magnetic Tweezers software interface. The next menu, “beads selection”, enables users to select a reference bead and a DNA-tethered bead by clicking on images of these beads and pressing the return key. The third “Calibration” menu triggers the collection of a series of images over a range of objective positions (focal planes) from the minimum to the maximum values specified in the objective control panel. These images are spaced 0.2 μm apart and serve to determine the extension of DNA. The rightmost menu “Clear Figures” clears and reinitiates data plotting in the left sub-panel of the data plotting panel.

The software was written in Matlab, therefore, any function can be terminated by pressing "Ctrl+C" in the Matlab command window and selecting "stop" in the "preview" menu. The software currently runs in Matlab2006b, and all the data are saved in directory C:\data\Magnetic Tweezers\experiment\. The folders are named with the date and time when the experiment begins.

§2.2 Design, produce and label DNA fragments

DNA fragments used in the projects were all produced using Polymerase Chain Reaction (PCR). The reaction mixture includes a DNA template (D. Lewis and S. Adhya, National Cancer Institute), nucleotide triphosphates (New England BioLabs, NEB), primers (Integrated DNA Technologies) and Taq DNA polymerase (NEB). Primers were used to setting the starting and end position for the reaction on DNA template to produce DNA fragments with the desired length and sequence.

§2.2.1 DNA fragments for Magnetic Tweezers experiments

DNA fragments about 3.2 kb in length were produced by PCR using the same plasmid DNA template (pDL2317) for both normal and 2,6-diaminopurine (DAP)-substituted DNA. For normal DNA we used dATP, dTTP, dCTP and dGTP, while instead, for DAP-substituted DNA, we use 2,6-diaminopurine -5'-Triphosphate (Trilink), dTTP, dCTP and dGTP in the reaction. The other components of the reaction remained the same. The PCR program for both normal and DAP-substituted DNA was: 95 °C for 3:00, 25 cycles of (94 °C for 1:00, 50 °C for 2:00, 72 °C for 6:00), 72 °C for 5:00, 55 °C for 3:00, and 37 °C for 3:00. The PCR product was purified using QIA quick Gel Extraction kit (QIAGEN) to eliminate excess

primers, nucleotides, and protein. This DNA fragment was digested with ApaI and SacII to produce overhangs on both ends. Since the pDL 2317 does not contain the cutting sites for ApaI and SacII, while the primers were designed to include those restriction sites, only amplified DNA fragments were digested. This scheme avoided contamination of DAP-substituted DNA with the normal DNA template. 1000 bp segments of bio- and dig-labeled DNA "tails" were produced by PCR with either 1:9 biotin- 11-dUTP : dTTP or 1:9 digoxigenin-11-dUTP: dTTP in the reaction mixture using template pBluKSP. This substitution resulted in approximately 5% labeling with biotin and digoxigenin in the DNA tails. The bio-tails digested by ApaI and dig-tails digested by Sac II were ligated to the sticky ends of the normal and DAP fragments using T4 ligase (NEB). Therefore, the resulting DNA fragment could attach to streptavidin-coated paramagnetic bead via the bio-tail and to the anti-digoxienin coated surface of the microchamber via the dig-tail.

§2.2.2 DNA fragments for EMSA

DNA fragments for EMSA experiments were produced by PCR reaction using the template pBR322 for both normal and DAP-substituted DNA. 200 base pair PCR products were digested with NgOMIV and AluI to eliminate incorporated primers leaving one sticky end with a 5'CCGG overhang and the other end blunt. The resulting 160 bp DNA fragment (929 – 1089 in pBR322) included the preferential cleavage site for *E. coli* gyrase at position 990 of pBR322. PCR and digested products were purified using QIA quick Gel Extraction kit (QIAGEN). Klenow Fragment (3' to 5' exo-, NEB) was used to label the DNA by adding Cy5-dCTP (GE healthcare) to base pair with base G in the sticky end. The molar ratio of Cy5-dCTP to DNA was about 10:1. Cy5 is blue fluorescent dye with excitation maxim at 649

nm and emission maxim at 670 nm. The labeled products were purified using QIAquick Nucleotide Removal kit from QIAGEN to eliminate free Cy5-dCTP.

§2.3 Visualize and quantify DNA and protein bands

§2.3.1 Agarose gel electrophoresis

For DNA fragments longer than 1000 bp, 1% agarose gel was used to separate DNA fragments by size. First 1 gram of agarose (EMD) was diluted in 100 ml 1x TAE buffer (diluted from 10x TAE buffer, Fisher Scientific), and then the mixture was heated to near boiling in a microwave oven to dissolve the agarose. 30 ml of the hot, transparent gel solution was poured into a rectangular casting tray. A comb was positioned at one end of the casting tray with enough solution to submerge at least half of the height of the teeth on the comb to form wells in the gel which solidified after around 20 minutes at room temperature. Then, the gel was submerged in an electrophoresis tank filled with 1x TAE buffer. To prepare DNA sample for the gel, we mixed 1 μl of 6x loading dye (Fermentas) with 2 μl DNA sample (from PCR or digestion) and 3 μl distilled water. DNA molecular weight markers were prepared by mix 1 μl of 6x loading dye (Fermentas) with 5 μl General Rule DNA ladder (Fermentas). The DNA marker and DNA samples were loaded into the wells of gel. Finally, the gel was run for half an hour at about 10V/cm. The gel was stained by transferring the gel into a solution of ethidium bromide (1 mg/L) and soaked for more than 1 hour. The DNA bands in stained gel were visualized by on a UV Transilluminator in a darkened room.

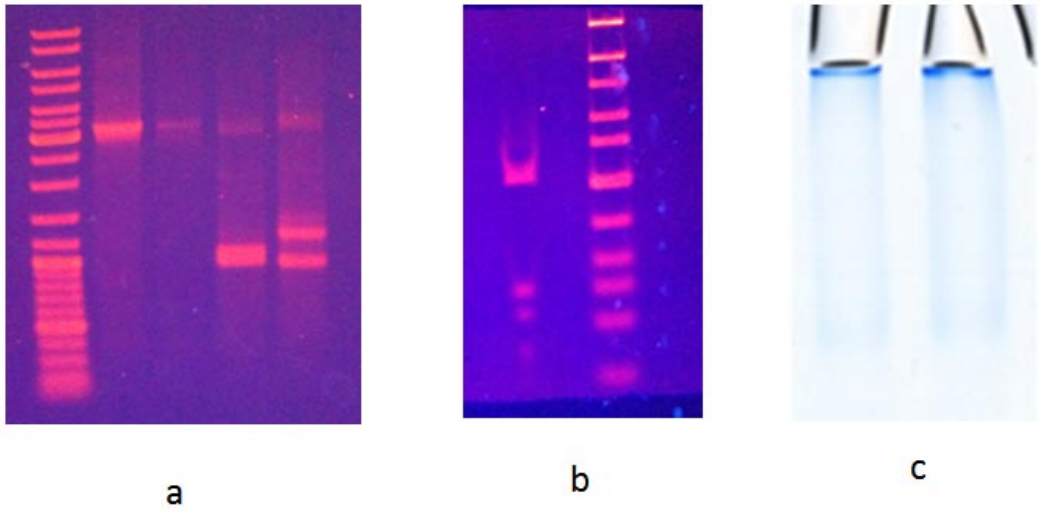

Figure 2.4 DNA and protein visualized in agarose and polyacrylaimde gels. An agarose gel stained with ethidium bromide (a): from right to left, 1kbp DNA ladder (NEB), 3.2 kbp normal DNA, 3.2 kbp DAP DNA, about 1 kbp bio-tail and dig-tail. A nondenaturing polyacrylamide gel stained with ethidium bromide (b): from right to left, 56 bp DNA with some fragment less than 20 bp, ultra low DNA ladder (NEB). Polyacrylamide gel stained with EZblue (Sigma) (c).

§2.3.2 Non-denaturing (native) polyacrylamide gel electrophoresis

4% native polyacrylamide gel electrophoresis was used for EMSA assays with DNA length less than 200 bp. A mini-PROTEAN II Electrophoresis Cell system was used to cast and run the gel. The gel was prepared by adding 1.5 ml 5x running buffer (0.5x TBE or 0.5x TB 5 mM $MgCl_2$), 1.5 mL 40% Acrylamide/Bis solution 37.6:1 (Bio-Rad), 75 µl 10% Ammonium Persulfate and 25 µl TEMED into12 ml distilled water in sequence. The mixture was quickly poured into the assembly of a pressed glass plate, and then a comb was inserted halfway into the gel to form wells. The 4% gel solidified in 1 hour. The glass plate assembly with gel was mounted on one side of the inner cooling core, the other side of the core was sealed by the

water dam, and then the complex was transferred into the gel tank. The gel tank was filled with running buffer to almost completely submerge the glass plate assembly. DNA samples were prepared and loaded following the same protocol as described for agarose gels. Finally, the protein –DNA mixtures were electrophoresed using 8 V/cm. Unlabeled DNA was stained using ethidium bromide for visualization with UV light. Instead DNA labeled with cy5 was visualized using a Typhoon Trio fluorescent scanner (GE Healthcare) with detection at 670 nm. Fluorescent bands corresponding to different DNA fragments were quantified using ImageQuant software (GE Healthcare).

Protein inside the native polyacrylamide gel was stained with Coomassie Brilliant Blue reagent (EZblue,Sigma) following the manufacturer's instructions. The blue bands of protein could be visualized directly with white light illumination.

§2.3.3 Use spectrophotometer to measure DNA concentration

To precisely determine DNA concentrations, a spectrophotometer was used to measure the DNA absorption spectrum. Double-stranded DNA has an absorption peak at 260 nm, which is routinely used to determine the concentration of DNA in solution using the Lambert-Beer Law: $A_{260} = \varepsilon * c * p$. In this equation, A_{260} is the amount of absorbance at 260 nm; ε is the molecule molar excitation coefficient with units of l/(mole cm); c (mole/l) is the molar concentration of the DNA, and p (cm) is the length of the light path through the sample. The width of the cuvette used was 1 cm, and ε was calculated according the DNA sequence using a tool called "UV spectrum of DNA" on the IDTdna website (http://biophysics.idtdna.com/UVSpectrum.html). We used the following method to determine the DNA concentrations for EMSA experiments. ε for the 200 bp DNA fragments (before restriction enzyme digestion) was 3180409 l/(mole cm) , and ε after digestion ε for

160 bp DNA was 2564320 l/(mole cm). Since the DAP nucleotide has a different extinction coefficients from adenine, the IDTdna "UV spectrum of DNA" tool was used to calculate the each ssDNA containing DAP and then the formula $\varepsilon_D = (1- h_{260nm})*(\varepsilon_1+\varepsilon_2)$ was used to calculate the excitation coefficient (ε_D) for dsDNA. In this formula, ε_1 and ε_2 are the excitation coefficient of each ssDNA, $h_{260nm}= 0.287f_{AT}+0.059f_{GC}$, and f_{AT} and f_{GC} are the percentage of AT and GC base pairs. ε_D for the 160 bp DAP DNA fragments was calculated to be 2411218 l/(mole cm). Using these extinction coefficients, measurements of A_{260} were used to determine the concentration of normal and DAP DNA in solution.

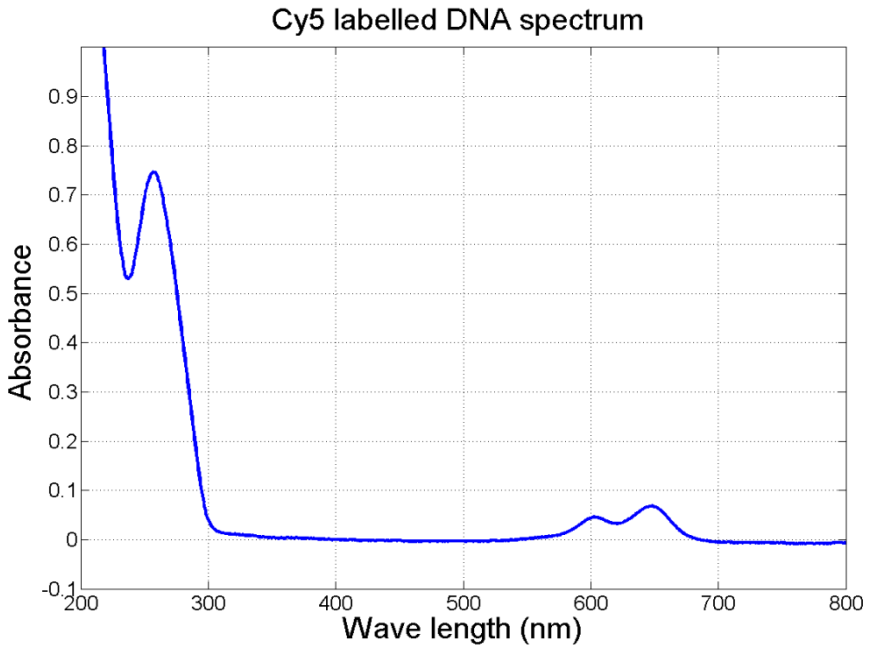

Figure 2.5 Spectrum of Cy5-labeled DNA. The spectrum shows peak at 260 nm (DNA absorption) and around 649 nm (Cy5 absorption).

In addition to DNA concentration, the labeling efficiency was also estimated by measuring the absorbance at 649 nm, the excitation maximum of Cy5. Since DNA almost has no

absorption at that wavelength, the concentration, *c*, estimated from the equation $A_{649} = \varepsilon * c * p$ (ε for Cy5 is 250000 l/(mole cm)) represented the concentration of Cy5-labeled DNA. A typical Cy5-DNA spectrum is shown in figure 2.5.

§2.4 Flow chamber design and preparation

Flow chambers were designed to allow buffer exchange during the experiment, in order to introduce type II topoisomerases and polyamines into the chamber. The first generation of flow chambers, shown in figure 2.6 a, was assembled using the following components to form a sandwich structure: a slide with holes drilled in each end, vacuum grease as spacer applied on the slide to form a rectangle space around the two holes, a cover slip sitting on the top of the grease secured by two strips of double sided tape. The cover slips and slides were cleaned with ethanol before assembling the chamber. The volume of the chamber is about 40 μl. In order to immobilize magnetic beads as references for the microscopy, 0.2 μl of 2.8 μm or 1 μm diameter paramagnetic beads (DYNAL M280 or MyOne beads coated with streptavidin 10 mg/ml) were diluted in 50 μl phosphate buffered saline (PBS) and drawn into the flow chamber. After at least 15 minutes incubation, the chambers were washed using 200 μl PBS buffer to remove beads floating in the chamber. 60 μl of 20 μg/ml anti-digoxigenin (Roche) was introduced into the chamber and incubated overnight at 4 degrees C°. Then the flow chamber was washed with 800 μl of PBS, and 80 μl BSA (100 μg/ml) was introduced and incubated for one hour. In parallel, 1 μl of paramagnetic beads were washed twice: first in 200 μl PBS and then in 100 μl PBS. These beads were diluted in 10 μl PBS and mixed with 2 μl of the DNA ligation product. This bead-DNA mixture was diluted in 300 μl of lambda buffer (10 mM Tis-HCl (pH 7.4), 200 mM KCl, 5% dimethyl sulfoxide (DMSO), 0.1 mM ethylenediaminetetraacetic acid (EDTA), 0.2 mM dithiothreitol) [80] .

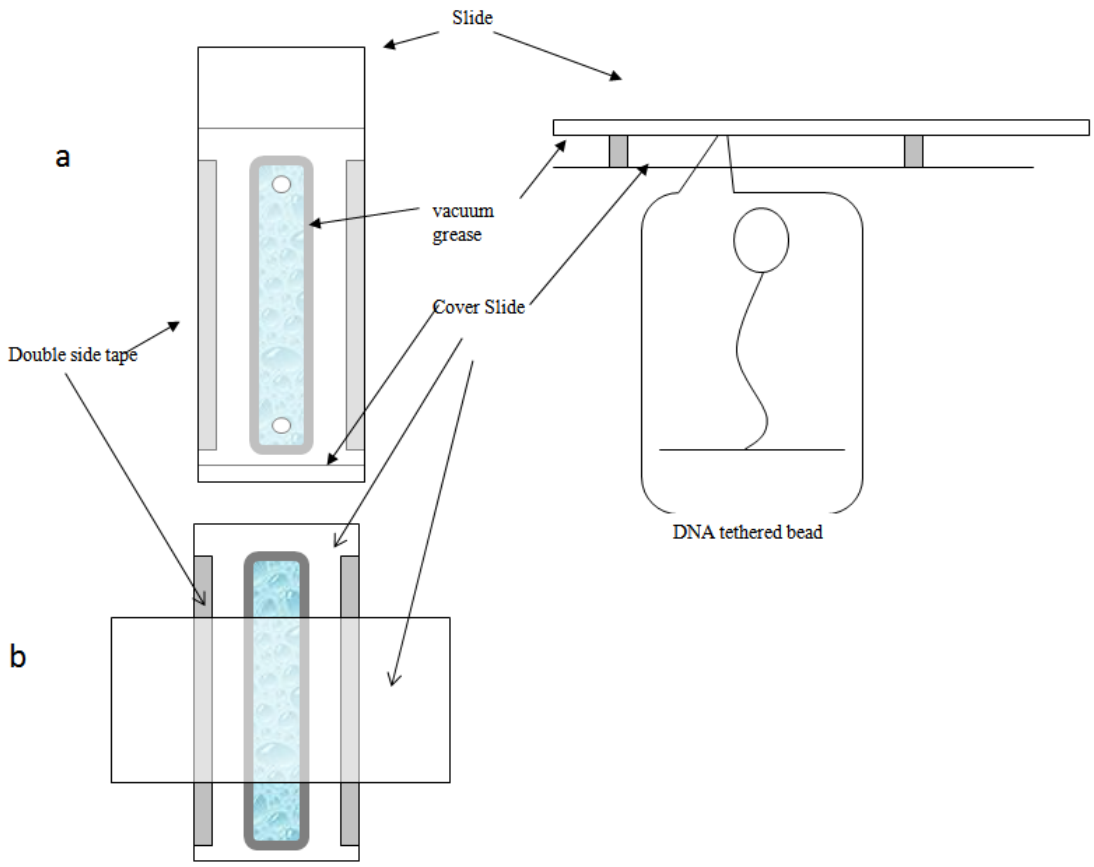

Figure 2.6 Two designs for flow chambers. A flow chamber in which lower forces were possible was made from a slide with two holes and a cover slip (a), while a flow chamber in which higher forces were possible was made using two cover slips (b).

The flow chamber was then washed with 800 µl lambda buffer, and the diluted beads and DNA mixtures were introduced and incubated for one hour before beginning an experiment. During experiments, solution can be used to wash out the unbound bead anytime on the microscope. A drawback of this design of flow chamber was that the minimum separation between the magnets and the tethered beads was limited by the thickness of the slide which limited the maximum tension that could be applied to the DNA tethers[73] . For the second generation of flow chambers, the slide was replaced with the second cover slip as shown in

the figure 2.6 b. This design increased the maximum force that could be applied from 1 pN to 20 pN for MyOne beads and from 20 pN to 70 pN for M280 beads.

§2.5 Experimental procedures

§2.5.1 Selecting a full length, dsDNA tether in Magnetic Tweezers

The flow chamber with DNA-tethered beads was mounted on the stage and brought into contact with the objective. After activating the Magnetic Tweezers software and selecting "Preview", a live video of the tethered beads appeared on the screen. Since the field of view only covered a very small part of the flow chamber, a search was necessary before a full length, unnicked DNA tether could be found beside a stuck bead that served as a reference. Then the magnets were lowered to a position at which the force was around 1 pN (17 mm magnet position for MyOne bead and 15.5 mm for M280 bead). Usually, the focus is adjusted to a plane above the DNA-tethered beads, therefore they are closer to focus than the reference beads and look smaller with fewer diffraction rings and more contrast as shown in figure 2.3.

Acceptable DNA tethers need to meet several criteria before starting an experiment. First of all a DNA tether should be the correct length. The length can be estimated by determining how far the focus must be changed to create similar images of a DNA-tethered bead and a bead stuck on the surface. This length should be approximately the expected contour length of the DNA in order to pass the test. A second test discards multiply tethered beads, since the paramagnetic beads have multiple biotin binding sites, and more than one DNA molecule may bind and tether a single bead. A single right-handed DNA helix only forms plectonemes and contracts at tensions larger than 1 pN if it is twisted in the direction of wrapping of the

helix. Instead double or triple DNA tethers form plectonemes and contracts when twisted in either direction.

A DNA tether that met both of these screening criteria was then examined further. After collection of a series of images for determining the *z* displacements, the DNA extension at low tension was monitored at different degrees of added twist to verify the symmetry of the plectonemic contraction as well as to find the position of maximum extension, ie. the torsionally relaxed state. Since the attachment points of the DNA tether and reference bead may not be at the same height if the slide is tilted or wedge-shaped, the "chapeau" curve can also be used to find the offset and correct measurements of the DNA extension. At high degrees of twist, the DNA extension will not change as a function of twist, because the extensive plectoneme in the DNA tether draws the bead almost to the surface of the chamber. The difference between this height and that of the reference bead reveals the height offset which must be corrected for in determining the DNA extension.

After that, a force calibration at different magnet positions is conducted. At each position, the data can be acquired at a rate about 20 frames/second for 10 seconds before moving to the next position. The extension, $l = \langle z \rangle$, of the molecule of the DNA was monitored with an error of about 10 nm with 200 frames averaging using three-dimensional, video-rate tracking of the bead. The horizontal motion of the bead $\langle \Delta y^2 \rangle$allowed the determination of the tension in the molecule via the equipartition theorem: $F = k_B T l / \langle \Delta y^2 \rangle$ with 90% accuracy. The force vs. extension data were fitted with worm-like-chain model to determine the persistence length of the DNA. Any spurious drift in the data was subtracted by referencing all positions to those of a second bead stuck on the surface nearby. For analysis a 10 second time filter data was applied to suppress the noise.

§2.5.2 Polyamines affect DNA supercoilings

Spermine was diluted in 200 μl λ buffer to final concentrations of 0.2mM, 0.5mM, 0.7mM, 1mM, and 2mM, and spermidine to final concentrations of 1mM, 2mM, 5mM, and 10mM. Solutions containing high concentrations of spermine (>0.5mM) and spermidine (>2mM) were required vortexing to avoid aggregation that obstructed flow into the chamber. Magnetic Tweezers (MT) were used to twist or untwist the DNA tethers at three different tensions, 0.2 pN, 0.6 pN and 1.0 pN, and at increasing concentrations of each of the two polyamines, spermine and spermidine. At 0.2pN, 0.6pN and 1pN, DNA were unwound from zero torsion point (0 turn) to -30 turns (corresponding to -10% supercoiling density (σ) for 3kbp DNA), rewound from -30 turns to 30 turns and unwound back to 0 turns in increments of 3 turns. The extension of each DNA tether was recorded as the function of turns during unwinding and rewinding.

DNA tension versus extension data was also collected for each concentration by using MT to stretch the tethers at tensions ranging from approximately 0.02 pN to 4 pN. Molecules were relaxed and stretched twice and their extensions were recorded as a function of tension during each cycle.

§2.5.3 Unwinding and rewinding normal and DAP DNA

Magnetic Tweezers were used to unwind and rewind DNA molecules under a range of tensions: 1.5 pN, 2 pN, 2.5 pN, 4.6 pN, 6 pN and 8pN. The DNA was attached in a flow chamber filled with λ buffer. At each force, DNA were wound from the zero torsion point (0 turn) to about 30 turns (corresponding to about 10% supercoiling density (σ) for 3kbp DNA), unwound back from around 30 turns to 0 turns measuring the extension every 3 turns. Then,

DNA were unwound from zero torsion point (0 turn) to about -700 turns (corresponding to > -200% supercoiling density (σ) for 3kbp DNA), rewound from around -700 turns to 0 turns every 20 or 40 turns. The extension of each DNA tether was recorded as the function of turns during unwinding and rewinding. DNA extension vs. turns data were also recorded at low force 0.25 pN to serve as control to be compared with the unwinding at much higher force.

The torsion-induced conformational change data were recorded by monitoring the extension of DNA during the following procedure: at 2.5 pN, DNA was unwound from 0 to -600 or -300 turns with rotational speed 15 turns/s, leaving DNA in negative supercoiled state for about 1 minute, and then rewound back to 0 turns at the same speed.

§2.5.4 DNA and Type II topoisomerases interactions

E. coli DNA gyrase (NEB) at varying concentration (184 nM -920 nM) was incubated with 40 nM of the Cy5-labeled, 160 bp double stranded DNA for 30 min at room temperature. The total volume of the reaction was 25 μl. Gyrase reaction buffer contained 35 mM Tris-HCl pH 7.5, 5 mM $MgCl_2$, 24 mM KCl, 2mM DTT and 10% glycerol [81]. Reactions were loaded directly onto a 4% native polyacrylamide gel in 45 mM Tris-borate and 5 mM $MgCl_2$ [82]. The gels run on ice for about 2 hours at 8V/cm, and DNA was visualized using a Typhoon Trio fluorescent scanner (GE Healthcare) with detection at 670 nm. The free and gyrase-complexed DNA bands were quantified using ImageQuant software (GE Healthcare).

Human topoisomerase II alpha (USB) was used at a final concentration of about 20 units/ml (200 ng/ml). *E. coli* DNA gyrase (NEB) was used at a final concentration of about 20 units/ml. The topoII and gyrase relaxation experiments were performed at 0.6 pN of tension in topoII buffer (50 mM Tris-HCl, 50 mM KCl, 8 mM $MgCl_2$, 1 mM EDTA, 0.5 mM DTT, pH=7.9 at room temperature) [83]. The flow chamber was washed using topoII buffer before

adding human topoII and DNA gyrase. ATP (USB) was added to the reaction buffer as indicated. The gyrase wrapping experiments were performed in gyrase reaction buffer (35 mM Tris-HCl, 24 mM KCl, 4 mM $MgCl_2$, 2 mM DTT pH=7.6 at room temperature) at 0.4 pN with 1 μm diameter, paramagnetic beads (DYNAL MyOne beads coated with streptavidin 10 mg/ml). Flow chambers were sealed with two little pieces of silicon gasket covering two drilled holes. Experiments were performed without evaporation from flow chamber for hours.

Chapter 3

Effects of polyamines on DNA supercoiling

§3.1 Outline

In this chapter I describe how two polyamines, spermine and spermidine affect the DNA supercoiling behavior at different tensions. In particular, I used Magnetic Tweezers to measure DNA extension as a function of added twist at various physiological concentrations of polyamines. The effects of the polyamines were characterized on both negative and positive supercoiling. Furthermore, we analyzed the data in the framework of a theoretical model developed by Dr. Goyal, a postdoctoral fellow in the group in order to extrapolate the geometrical parameters of the supercoil loops. My observations suggest that polyamines tend to stabilize the right-handed, double stranded B-form of DNA and promote plectoneme formation. Furthermore, my calculations quantitatively reveal the compaction of plectonemes at physiological concentrations of the two polyamines. I found that an order of magnitude less tetravalent spermine produces the same level of compaction as the trivalent spermidine.

§3.2 Experimental results and analysis

Figure 3.1 shows DNA extension versus added twist turns for a representative DNA tether at various physiological concentrations of spermine (left column) and spermidine (right column). The number of turns has been normalized as $\sigma = (Lk - Lk_0)/Lk_0 = n/Lk_0$, where Lk_0 called linking number is the number of right-handed helical turns in the torsionally-relaxed state of B-form dsDNA, and n is the number of rotations added to the DNA. σ is a measure of the "supercoiling density". Likewise, z is the DNA extension normalized to the contour length, L, of DNA. I investigated the effect of polyamines on DNA extension versus twist at three different tensions, 0.2 pN (first row in Fig. 3.1), 0.6pN (second row) and 1.0 pN (third row). The blue curves represent the DNA in the absence of polyamine, or "control DNA".

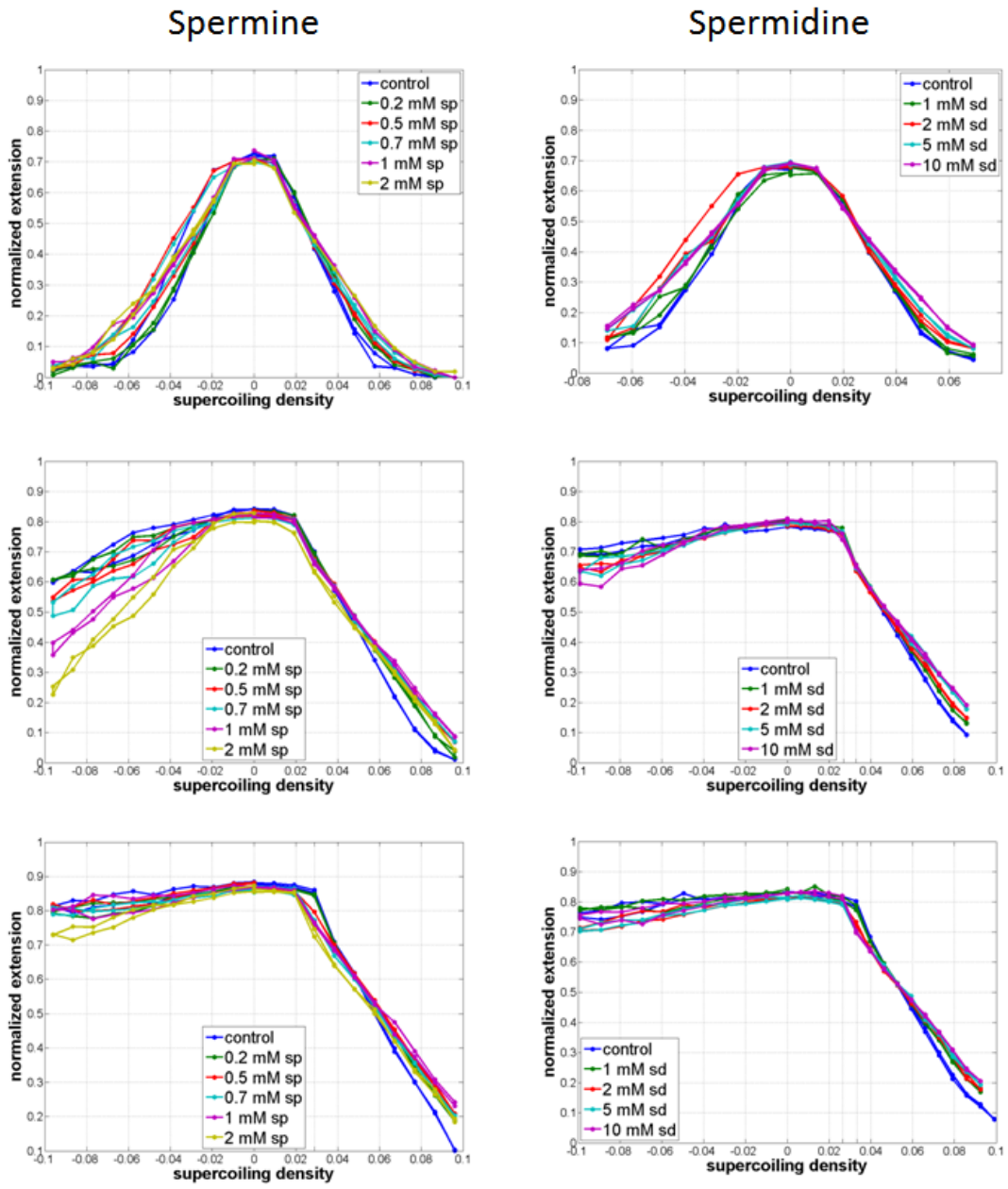

Figure 3.1 DNA extension vs. supercoiling density at different concentrations of spermine (left column) and spermidine (right column). The top curves were obtained at 0.2 pN, the middle at 0.6 pN and the bottom at 1.0 pN. The spermine concentrations are 0 mM, 0.2 mM, 0.5 mM, 0.7 mM, 1 mM and 2 mM. The spermidine concentrations are 0 mM, 1 mM, 2 mM, 5 mM and 10 mM. The data are shown for a representative DNA molecule for each polyamine.

Before interpret the effects of the two polyamines on DNA supercoiling from the data, let me review the known behavior of DNA without polyamines at the three different tensions (refer to the blue curves). I will do so, by explaining the “knee points" on the blue hat curves and their nearly straight line part on the positive side of σ.

At all tensions, as I over-twist DNA, its extension initially decreases only slightly and then drops sharply going past a “knee point” on the curve. This is explained as follows. A filament that has some stiffness in bending and torsion, “buckles” at a critical value of twisting , n_b, and collapses to form plectonemes (where the axis of the double helix intertwines and forms a superhelix). Such dynamic buckling has recently been simulated using rod mechanics [84], and was also detected in single-DNA molecule experiments [27]. Thus, as we over-twist (wind) DNA, beyond a threshold, its extension starts falling sharply with more and more length of DNA getting absorbed in the plectonemic branch. In thermodynamic equilibrium, the transition to the plectonemic state from the stretched state must be governed by the free energy competition between the two states, and is expected to be observed sooner than the mechanical buckling point, n_b as explained in Fig. 3.2 . The knee point of the extension versus twisting-turns curve is occurs at a critical number of turns, n_{cr}, at which the free energies of the two states become equal. This critical point increases with the tension.

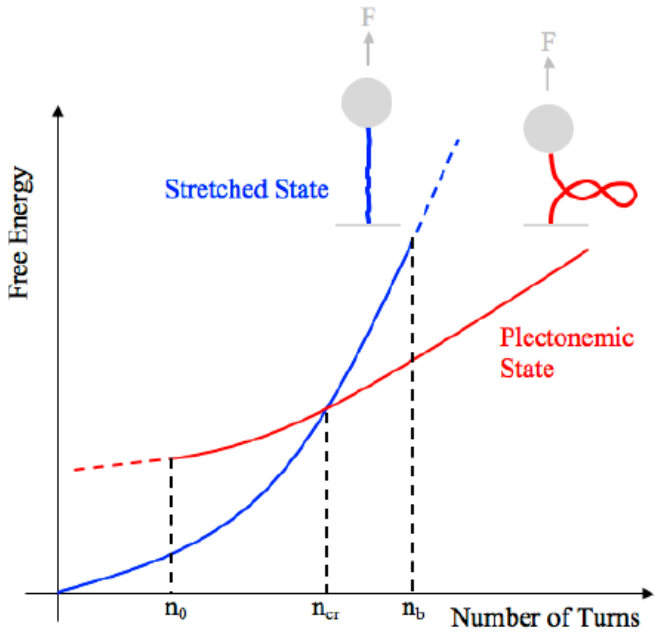

Figure 3.2 A qualitative sketch showing free energy competition between the plectonemic and stretched states of DNA in extension versus twisting experiments. Solid curves correspond to “stable mechanical equilibria", while the dashed curves correspond to “unstable mechanical equilibria". Thermal fluctuations at a fixed value of n chosen between n_0 and n_b allow DNA to jump back and forth between the two stable mechanical equilibria. Note that an unstable mechanical equilibrium can not correspond to a thermodynamic equilibrium. So, n_0 is the earliest point, at which a plectonemic state can be detected in the single-molecule twisting experiments. By the same token, the interval $[n_0; n_b]$ is the transition interval from a DNA always in the stretched state (at $n < n_0$) to stretched DNA in the plectonemic state (at $n > n_b$).

Also, notice that at the low tension of 0.2 pN, the “extension versus supercoiling density” curves for control DNA (blue) in Fig. 3.1 have the same qualitative trends for both positive and negative σ. However, at 1 pN, the blue curve is nearly horizontal for negative σ, suggesting that plectonemes do not form. Perhaps, during unwinding at high tension, disruption of the right-handed B-form is energetically more favorable than plectoneme formation. Finally, at an intermediate tension of 0.6 pN, the blue curve shows an asymmetric

trend about the σ = 0 axis; the slope on the negative side of the curve is less steep than on the positive side. This may be explained by assuming that some disruption of the B-form structure of DNA occurs along with plectoneme formation.

Next, let us explain the nearly straight line parts of the blue curves for positive σ. Once the first plectoneme is nucleated and is sufficiently large, it has been shown from simplistic rod theories [28, 29] that the linking number added via bead rotation almost completely translates into writhe, keeping the twist constant. Thus, this behavior resembles a phase change scenario, wherein more and more length of DNA gets absorbed into the plectonemic phase at a constant twist. If each additional writhe consumes the same length of DNA, then the extension of DNA tether must fall at a constant rate with added twisting, resulting in the observed straight line. Furthermore, the slope of this straight line indicates the number of DNA bps in a plectonemic loop. The steeper the slope is, the more bps in each writhe, and hence less compact is the plectoneme.

In the next sections, I will discuss the changes that polyamines make to the "extension versus supercoiling density" curves. Notice that spermidine needs to be added in higher amounts than spermine to observe similar effects, also note that the bending persistence length estimated by fitting worm-like chain model on DNA extension versus force data appears unchanged with increasing concentration of polyamine.

§3.2.1 Spermine and Spermidine stabilize right-handed B-DNA

The data in Fig. 3.1 indicate that spermine and spermidine stabilize the right-handed B-form of dsDNA structure. This is most evident in the plots in the middle of Fig. 3.1, which show DNA extension versus supercoiling density at 0.6pN. For negative σ, the B-form of dsDNA

may disrupt and/or form plectonemes. The decrease in the extension of DNA with added negative turns must correspond to writhe. The remaining torsional stress must induce an alteration in the B form of DNA that does not cause a decrease in extension. Increasing the spermine or spermidine concentration increases the magnitude of the slope on the negative side of the hat curve indicating that plectoneme formation becomes a preferred pathway for relief of torsional stress. Thus, this observation corroborates the notion that B-DNA duplex structure is stabilized in the presence of spermine and spermidine. A direct physiologically relevant corollary of this effect is that spermine and spermidine make plectoneme formation favorable in negatively supercoiled DNA, which is always adopted in bacterial plasmid [50].

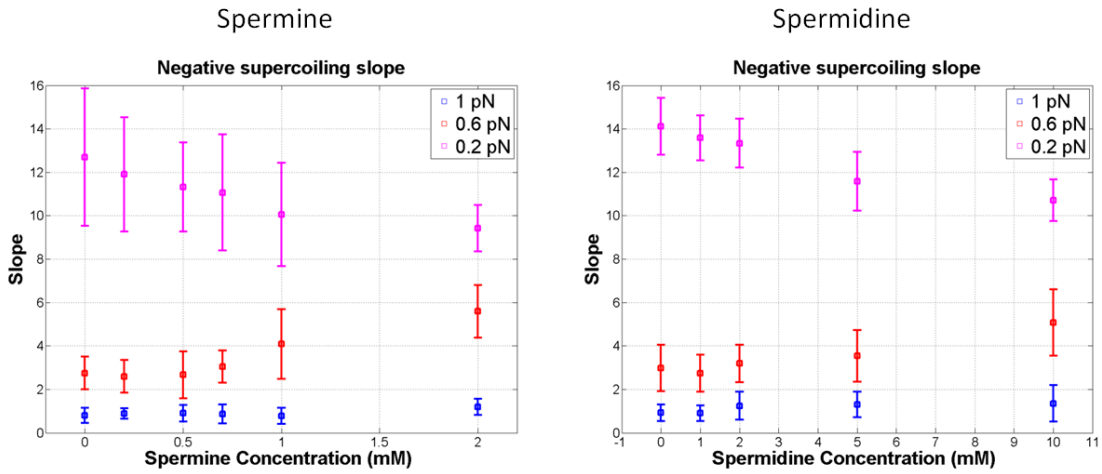

Figure 3.3 Effect of polyamine concentration on the slope of hat curve for negative supercoiling. Each point represents the average over eight DNA tethers, as a function of spermine (left) and spermidine (right) concentrations at 0.2 pN, 0.6 pN and 1pN. Error bars represent standard deviations.

In order to understand the effect described above quantitatively, I plotted the average slope of negative supercoiling part for all the three tensions as a function of increasing concentrations

of spermine and spermidine (Fig. 3.3). At 0.6pN, there is a noticeable increase in the slope indicating how favorable plectoneme formation is compared to the deformation of B-form DNA. The steeper the slope is, the more stable the DNA duplex is during unwinding at the highest concentrations used are 2 mM for spermine and 10 mM for spermidine. However, it may be possible that at higher concentrations of polyamines, the magnitude of the negative supercoiling slope becomes equal to the magnitude of the positive supercoiling slope, making the hat curve symmetric. At 0.2 pN, the curves are symmetric. Therefore, the decrease in slope must correspond to formation of more compact plectonemes which consume a smaller number of DNA base pairs. At 1 pN, there is hardly any change in the slope because it is close to zero indicating that the tension is high enough to prevent any plectoneme formation.

§3.2.2 Spermine and Spermidine promote plectoneme formation

The two polyamines also seem to facilitate formation of plectonemes which initiates at lower value of supercoiling density. This is seen by noticing the value of σ at which DNA extension first drops (Fig. 3.1). I named this value of σ as the "observed transition point", and note that it may be in close proximity of n_{cr} depicted in Fig. 3.2. I found that the observed transition point decreases with increasing polyamine concentration. This effect is particularly visible at high tensions (1 pN and 0.6 pN). The observed transition points at these forces are plotted as a function of increasing spermine and spermidine concentrations in Fig. 3.4. At the smaller tension of 0.2 pN, these effects were not detectable because of the fluctuation in DNA extension.

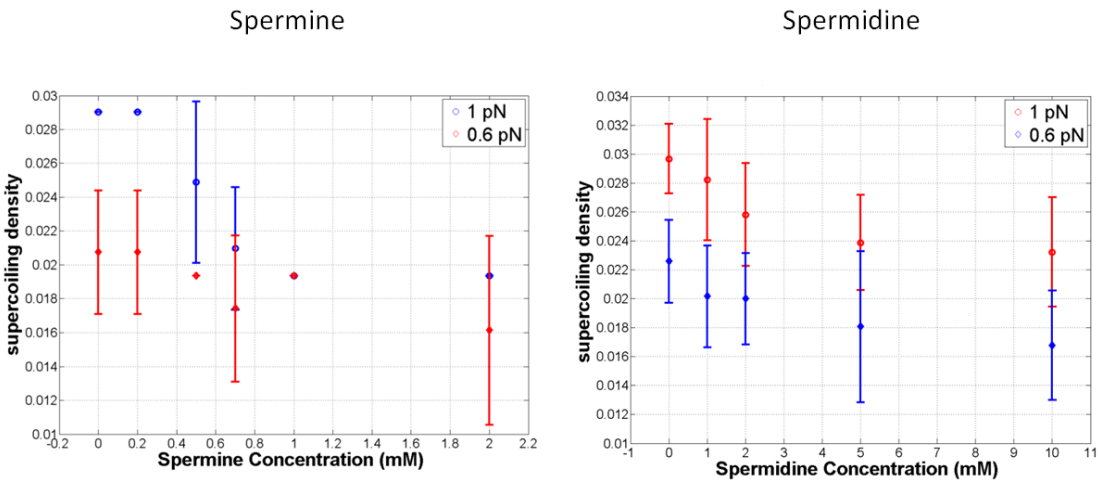

Figure 3.4 Effect of polyamine concentration at 1 pN and 0.6 pN on the observed transition points. As the concentration of polyamines was increased, plectonemes began to form at lower supercoiling densities. Error bars represent standard deviations.

§3.2.3 Spermine and Spermidine shrink plectonemic supercoils

Figure 3.5 shows the average magnitude of the post-buckling slope as a function of spermine or spermidine concentration when DNA has been wound (i.e. when σ is positive). The magnitude of the post-buckling slope decreases with increasing polyamine concentration. The slopes are shown for all three values of tension, 0.2 pN, 0.6 pN and 1 pN. Recall that the slope represents how many bps of DNA are contained in a plectonemic loop. Therefore, a larger slope will correspond to a bigger plectonemic supercoil. In Fig. 3.5, we observe that as the polyamine concentration increases, the slope reduces and tends to reach asymptotically a constant value. This observation directly indicates that the plectonemic supercoil shrinks with increasing concentration of polyamine. Furthermore, the slope trends indicate that the plectonemes are more compact at higher tensions. However, the compaction of plectoneme due to the polyamines is most pronounced at low tension. In order to analyze the plectoneme

compaction quantitatively, we used simple elastic rod theories to calculate the writhe density and plectonemic radius from the slope as described below in Section 3.3.

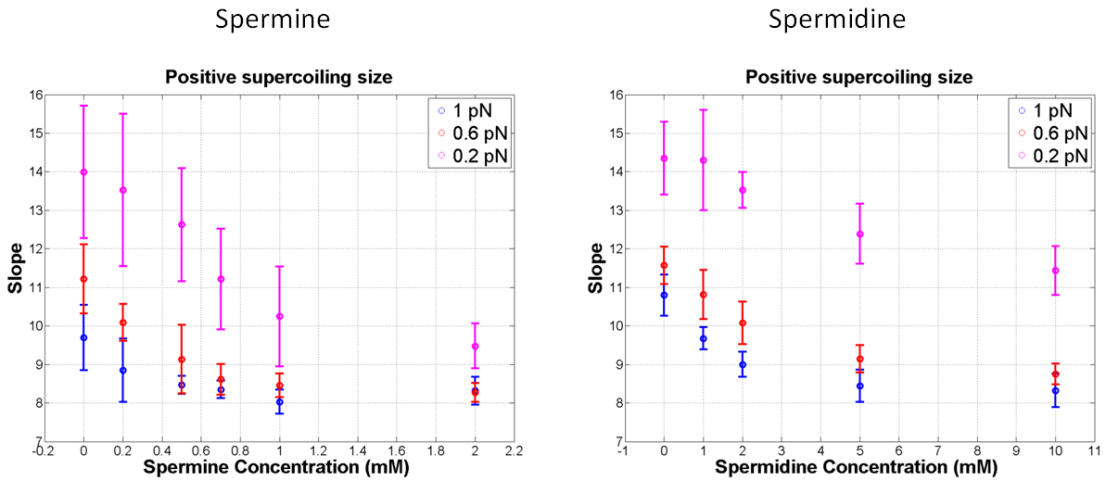

Figure 3.5 Slope of the positive supercoiling part of the hat curve. Each data point is the average of eight DNA tethers, at different spermine (left), or spermidine (right) concentrations, and at 0.2 pN, 0.6 pN and 1pN. Error bars represent standard deviations.

§3.3 Calculations of the plectoneme condensation

In this section, we calculate how each of the two polyamines affects the topological features of the plectonemic phase. In particular, we calculate writhe per helical turn and radius of the plectoneme as a function of increasing polyamine concentrations at 0.6 pN and 1.0 pN tensions. We assume that the plectonemic phase consists of two identical double helices with opposite orientation, with uniform radius R and uniform helical angle α, and ignore the end loop [29]. Assumption of a uniform helical angle, has been analyzed [28] and seems legitimate. Furthermore, it is also assumed that any turn, n, added after the buckling transition,

completely translates into writhe, Wr, leaving the twist unchanged. This means that more DNA becomes involved in the plectonemic phase without any change in the features of the plectonemic phase. With these assumptions, from the analysis in [29] that the writhe density in the plectonemic phase is inversely proportional to the slope given in Fig. 3.5. In particular writhe per helical turn in the plectonemic phase is given by

$$\left|\frac{W_r}{Lk_0(l_p/L)}\right| = \rho_{th}\left|\frac{dz}{d\sigma}\right|^{-1} \qquad \textbf{[Eq.3.1]}$$

where z is the extension normalized to the contour length L of DNA, σ is the number of turns, n, added to DNA normalized to the linking number Lk_0 of the torsionally relaxed DNA, $\boldsymbol{l}_{\boldsymbol{p}}$ is the length of DNA absorbed into plectonemic phase, Wr is the writhe and ρ_{th} is the contraction factor due to thermal fluctuations. It is assumed that the thermal fluctuations are predominantly in the stretched phase of DNA.

The slope $\left|\frac{dz}{d\sigma}\right|$ is available from Fig. 3.5 and the contraction factor ρ_{th} in the stretched phase can be approximated using the Moroz and Nelson approximation for a twisted fluctuating filament [30] for tensions > 0.5 pN as follows:

$$\rho_{th} \approx 1 - \frac{1}{2}\frac{1}{\sqrt{\frac{K_b F}{{k_B}^2 T^2} - \frac{{M^2}_{3(cr)}}{4{k_B}^2 T^2} - \frac{1}{32}}} + \frac{K_b k_B T}{L(K_b F - \frac{{M^2}_{3(cr)}}{4})} \qquad \textbf{[Eq.3.2]}$$

Where,

$$M_{3(cr)} \approx \sqrt{2K_b F} \qquad \textbf{[Eq.3.3]}$$

is the restoring torsional moment exerted by the twisted DNA on the bead, K_b is the bending stiffness, F is tension, k_B is the Boltzmann constant, and T is the absolute room temperature. Note that as plectonemes begin to form, the torsional moment saturates [27].

To complete the calculation of ρ_{th}, and hence writhe density, we need the bending stiffness, K_b. We fit the DNA extension versus force data at $\sigma = 0$ with the worm-like chain model [25] to estimate the bending stiffness, K_b

$$\frac{F}{k_B{}^2 T^2} = \frac{1}{K_b}\left[z + \frac{1}{4(1-z)^2} - \frac{1}{4} \right] \qquad \textbf{[Eq.3.4]}$$

Figure 3.6 shows the persistence length, which is proportional to the bending stiffness, as a function of polyamine concentration. Note that these experiments are not able to resolve any clear trends in bending stiffness as a function of polyamine concentration. Nevertheless, solving Equations (3.1 – 3.4), the writhe per helical turn may be obtained as a function of polyamine concentration as shown in Fig. 3.7. Observe that the polyamines can increase the writhe density to as high as 10%. This must result in a commensurate decrease in twist density. Therefore, a direct corollary is that polyamines tend to decrease the twist density by condensing the plectonemes.

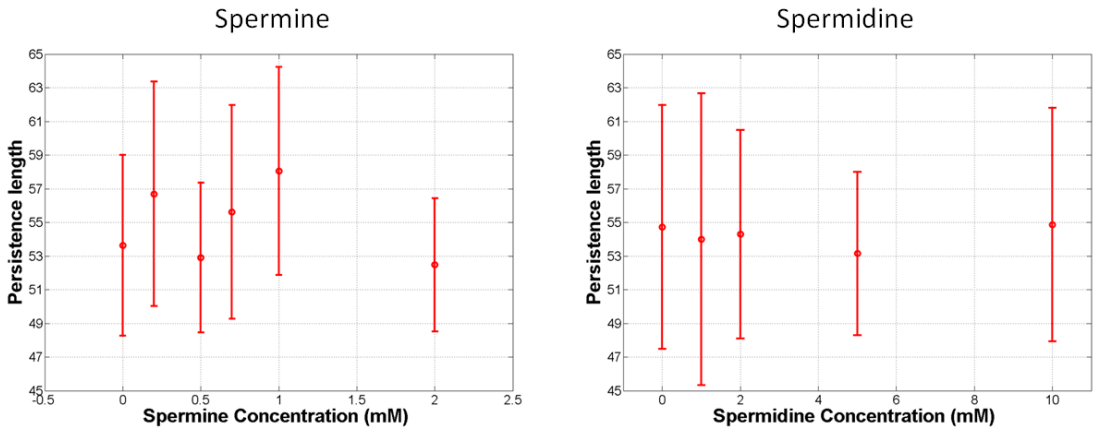

Figure 3.6 Persistence length (bending stiffness) vs. polyamine concentration. Each data point is the average over eight tethers. Error bars represent standard deviation. Bending stiffness of DNA appears unchanged with polyamines.

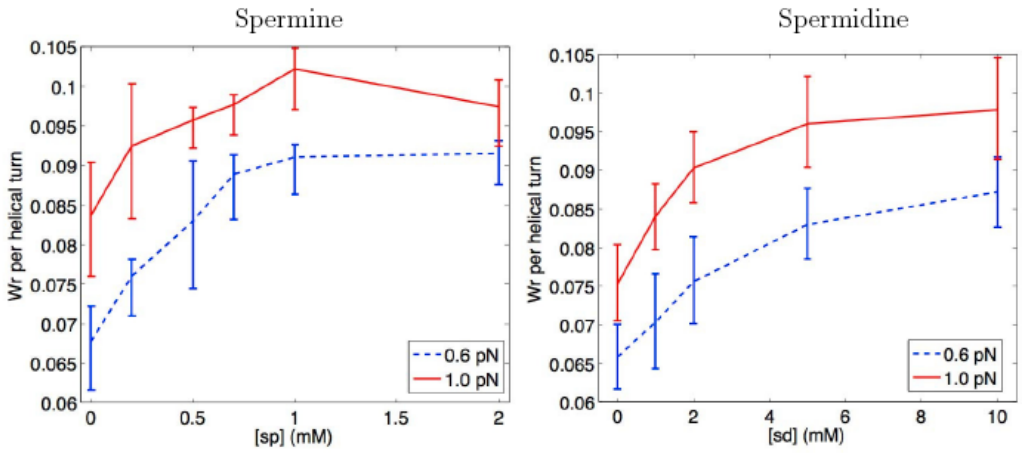

Figure 3.7 Writhe per helical turn in the plectonemic phase as a function of polyamine concentration. Increase in writhe density is a quantitative measure of plectoneme shrinking.

Finally, we calculated the radius, R of the helical plectoneme from the writhe formula of a helix,

$$R = \frac{\sin(2\alpha)}{4\pi}\left|\frac{W_r}{l_p}\right|^{-1} \qquad \textbf{[Eq.3.5]}$$

Assuming the helical angle $\alpha \approx \frac{\pi}{6}$ [29], we use Eq. 3.5 to get R versus polyamine concentration as shown in Fig. 3.8. The radius shrinks more substantially with polyamines at the lower force than at the higher force, yet it remains sufficiently larger than the radius of DNA.

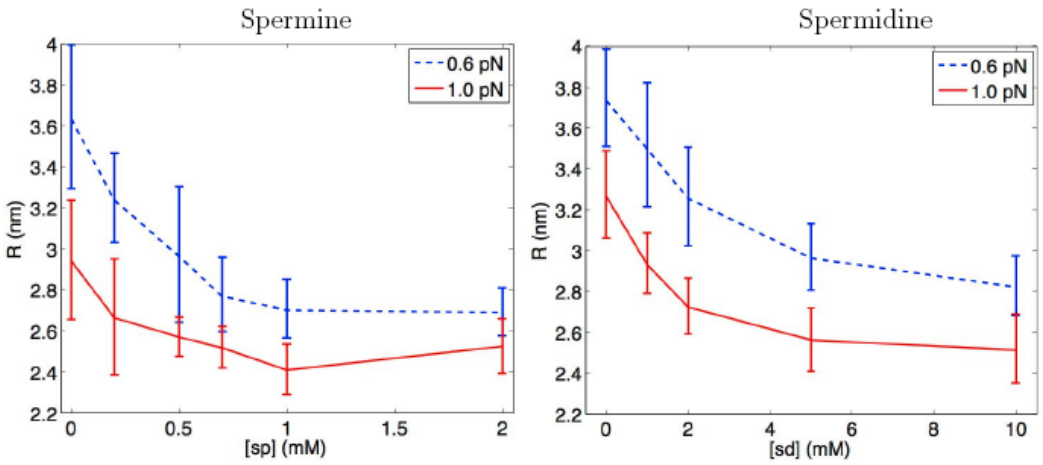

Figure 3.8 Radius of the plectoneme as a function of polyamine concentration. The radius shrinks substantially at low force.

§3.4 Discussion

To calculate the shrinking of the plectoneme radius, we assumed the helical angle remained the same at all forces and polyamine concentrations. However, note from Eq. 3.5 that the radius decreases as the helical angle decreases. It is known from simple rod mechanics models that the helical angle decreases slightly as the force decreases. However, drawing conclusions from such trends and Eq. 3.5, one may expect that the plectoneme radius will necessarily be smaller than what is shown in Fig. 3.8 as the polyamine concentration increases. Furthermore, at low force, the radius will be even smaller. The shrinking of plectoneme size is very important to facilitate the condensation of DNA by polyamines. In the experimental conditions I used, the high concentration of monovalent cations results in a nearly complete neutralization of the negative charges on the DNA backbone, thus DNA is electrostatically screened by the salt cations, and the addition of polyamines will not affect electrostatic interaction significantly. This screening effect can be used to explain why DNA condensation did not happen and the persistence length did not change with increasing polyamines concentration.

Any interpretation of how polyamines stabilize the DNA duplex structure should consider what kind of conformational change may occur in DNA while unwound at relatively high force. The most common explanation is that AT rich regions denatured to absorb the torsional energy [11], so the extension of DNA remains almost constant. The crystal structure and infrared spectrum of polyamie-DNA complexes [12, 85] show that spermine and spermidine could establish hydrogen bonds with bases from complementary strands of the DNA duplex, which bridge the two strands. Therefore, spermine and spermidine stabilize DNA against local denaturation induced by unwinding, and promote writhe. A different explanation

invokes local transition from right handed to left handed structure, instead of local denaturation. According to this view, the increase in torsional stress will trigger GC rich region to transit to left handed Z DNA, as a mechanism to absorb the decreasing of linking number [17]. This transition requires rotation of the base pairs along the DNA. This disrupts the major and minor grove structure in B-DNA. Instead of severe local conformational change, it is also possible that only twist density (or helical pitch) of DNA molecule will decreasing along the duplex when unwound. The decreasing of twist density will also affect conformation of major and minor grooves of DNA due to the change of helical pith of the DNA. Raman and energy minimization study indicate spermine and spermidine prefer binding along the major and minor grooves of DNA duplex, respectively [57, 86] . These specific binding modes will stabilize the conformation of the major and minor groove in B-DNA to prevent B to Z transition as well as significant decrease of twist density.

Once DNA starts to form plectonemes, the twist density will remain constant along the DNA molecule. Therefore, this result indicates that polyamine-bound DNA is less prone to change its twist density than unbound DNA. The higher the polyamine concentration is, the less prone DNA is to increase its twist density. In this way, the binding of polyamines to DNA modify the mechanical properties of DNA in response to torsional stress.

The ability of polyamines to suppress DNA helical distortion has great biological relevance. Most DNA binding proteins recognize the helical structures of DNA, ie. the minor groove or the major groove. Distortion of the DNA helical structure will inhibit or decrease the binding ability of those proteins. Polyamines could help preserving DNA helical structure against torsional stress introduced in the molecule as a consequence of cellular processes. There is

also a group of proteins known to separate the two strands in the DNA double helix, such as helicases. Binding of polyamine on DNA could interfere with the activity of these proteins. Therefore, polyamines could be one of the regulatory mechanisms the cell employ to control certain physiological activities. The fact that the levels of polyamines vary and are highly regulated during the cell cycle supports this idea.

Chapter 4

Behavior of DAP DNA under tension and torsion

§4.1 Outline

In this chapter, I will introduce the 2,6 Diaminopurine (DAP)-substituted DNA molecule. As mentioned in chapter 1, DAP substitutes for adenine and forms three H bonds with thymine instead of the two that form between AT base pairs shown in figure 4.1. The first part of this chapter describes the chemical structure and properties of DAP as well as DAP DNA. Since this base substitution probably affects base pair stacking interactions in dsDNA, I used Magnetic Tweezers to compare the mechanical properties of DAP DNA under tension and torsion with those of regular DNA. Indeed, DAP DNA can serve as a model system to study how base pair stacking energy contribute to the stiffness of DNA. Finally, because of the similarities between DAP:T and G:C base pairing in terms of number of H bonds, I used DAP DNA as a model system to investigate the effect of H bonds on the transition of the DNA double helix from a right-handed to left-handed structure at high levels of negative supercoiling (unwinding).

§4.2 Chemical structure and properties of DAP DNA

Compared to adenine, DAP has an extra exocyclic amino group on the 2 position instead of hydrogen (Fig. 4.1). This extra amino group is available for H bonding with the electronegative oxygen atom on thymine, thus a third H bond can form between DAP and thymine which makes this type of base pair very similar to a GC base pair. Furthermore, the exocyclic amino groups of DAP:T base pairs are located in the DNA minor groove. So, the DAP:T melting temperature and the width of the minor groove at this base pair are very close to those of a G:C base pair (Fig. 4.1 and ref. [87]). The overlap of the electrons perpendicular to the base pair plane contributes to the base pair stacking interactions. These electrons are

those from p orbital in the pyrimidine and purine ring systems as well as the lone pair of electrons from the oxy and amino groups. The extra nitrogen in DAP:T in the exocyclic amino group contributes one more pair of electrons to the stacking interaction than that of A:T base pair. Moreover, the extra H bond also contributes to the stability and stiffness of DAP:T base pair.

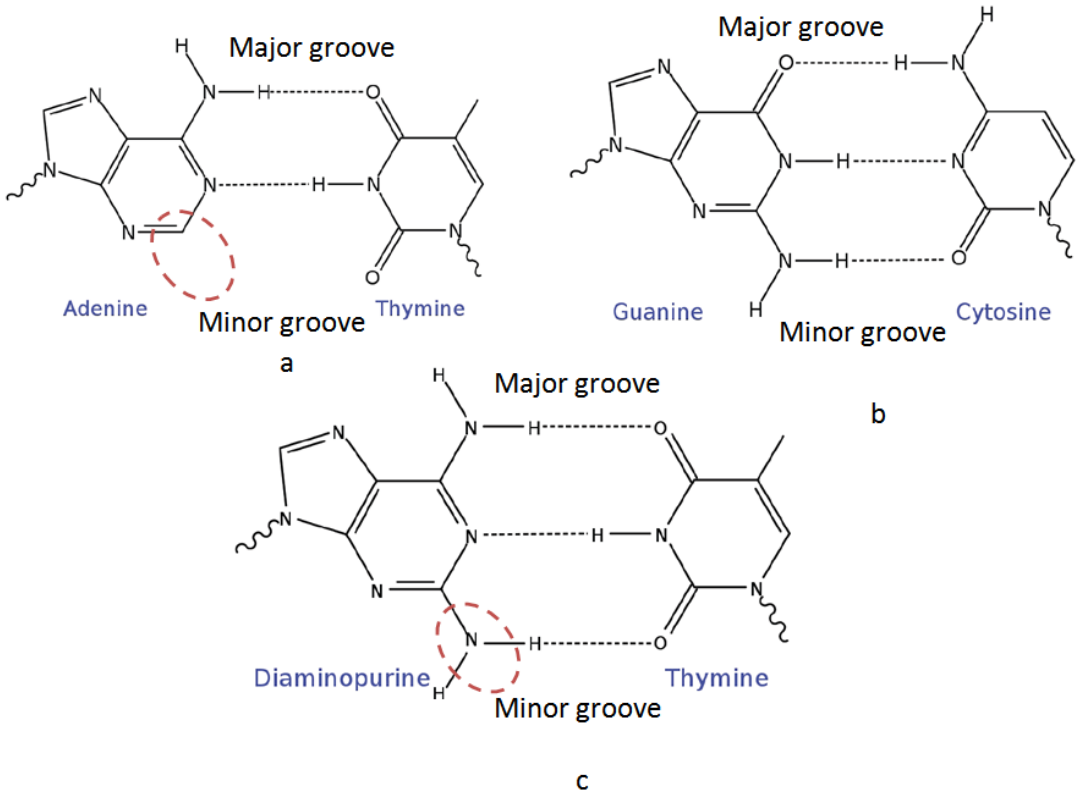

Figure 4.1 illustrations of A:T, G:C and DAP:T base pair. Dash circle highlights the extra exocyclic amino group in diaminopurine.

An NMR study showed that DAP-substituted, 10 bp-long DNA maintains the B-form [46]. Furthermore, I found that the polymerase chain reaction (PCR) and restriction enzyme digestion may be conducted on DAP DNA. Therefore, DAP DNA is a viable tool to investigate how changing the mechanical properties of the DNA affects its structural and functional characteristics.

§4.3 DAP-substituted DNA is stiffer

I used Magnetic Tweezers to investigate the physical properties of DAP-substituted DNA. Since Magnetic Tweezers can not only apply force but also torque, I could characterize the behavior of DNA under tension and torsion. I conducted MT measurements on 3.2 kb-long normal DNA and DAP DNA, ligated at their extremities to 0.9 kb DNA fragments multi-labeled with either digoxigenin or biotin as mentioned in chapter 2 materials and methods. (Fig. 4.2). Normal DNA is used, prepared and investigated in the same conditions as DAP DNA. In order to obtain the persistence length which represents the bending stiffness of DNA, I measured the end-to-end distance of the tethered DNA as a function of applied force and fit the force –extension curves with the wormlike chain model (1):

$$F = \frac{k_B T}{P}\left[\frac{1}{4(1-z/L)^2} - \frac{1}{4} + \frac{z}{L}\right] \qquad \textbf{[Eq.4.1]}$$

Where k_B is Boltzmann's constant, T is the temperature, P is the persistence length and L is the contour length of the DNA, z is the end-to-end distance measured from the experiments. The fitting persistence length of normal DNA is 52 ±10 nm (data obtained by averaging the fitted persistence length of 40 DNA molecules), which is consistent with previous measurements. In my measurements, the force vs. extension curves of DAP-substituted DNA

can also be fitted by the wormlike chain model. These results indicate that DAP-substituted DNAs share a structural similarity with normal DNA. However, the persistence length for DAP-substituted DNA, as derived from the fitting is 70 ±14 nm, which is much larger than that of normal DNA (Fig 4.2 a). Therefore, DAP-substituted DNA seems to be stiffer than normal DNA, in agreement with what was found for short DAP DNA fragments [45]. In order to confirm this observation, I also investigated the behaviors of both types of DNA under torsion (Fig 4.2 b). Since DNA is a right-handed double helix, when the molecule is rotated clockwise, the molecule is wound.

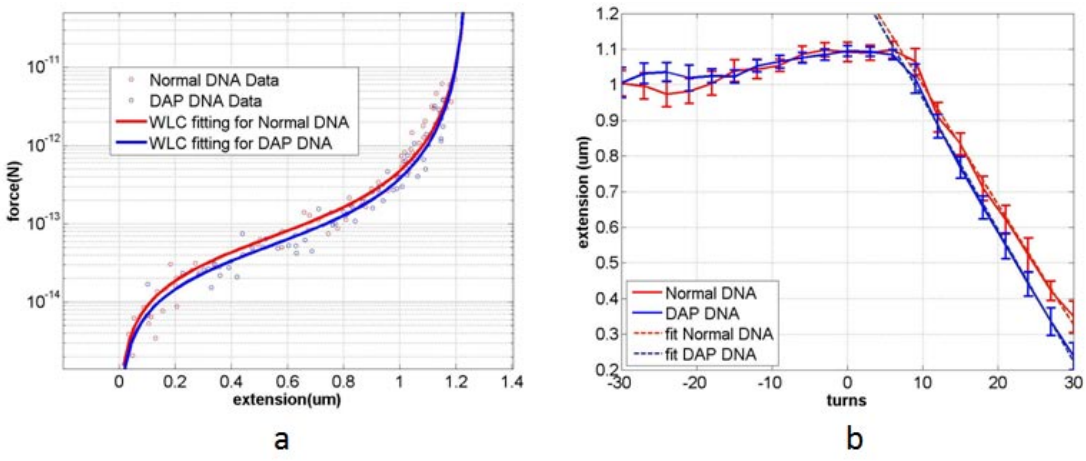

Figure 4.2 Normal DNA and DAP DNA behavior under tension and torsion. a. The worm like chain model fits the force vs. extension data for normal DNA (red) and DAP DNA(blue) ; b. Hat curve (extension vs. turns) at 0.6 pN for normal DNA (red) and DAP DNA (blue). A linear fit is applied on the linear regions of positively supercoiled DNA. The slope of the fitted lines indicates the supercoil size of the DNA.

This is indicated by positive numbers of turns imparted to the DNA molecule (right part of x-axis in figure 4.2). As a result of turning the molecule, twist initially builds inside the molecule without shortening the end-to-end distance. After a critical number of turns

supercoils start to form, and the end-to-end distance decreases linearly with the number of turns applied on the DNA. I measured the slope (equivalent with the length of DNA involved in each supercoil) of the DNA extension vs. turns curve in the plectonemic region. The slope for DAP-substituted DNA (36.1±2.4 nm/turn) is larger than that of normal DNA (33.8±3.7 nm/turn) (Fig. 4.3), which indicates that a loop in a DAP DNA supercoil is bigger than in normal DNA. These findings support the results that DAP-substituted DNA is stiffer than normal DNA.

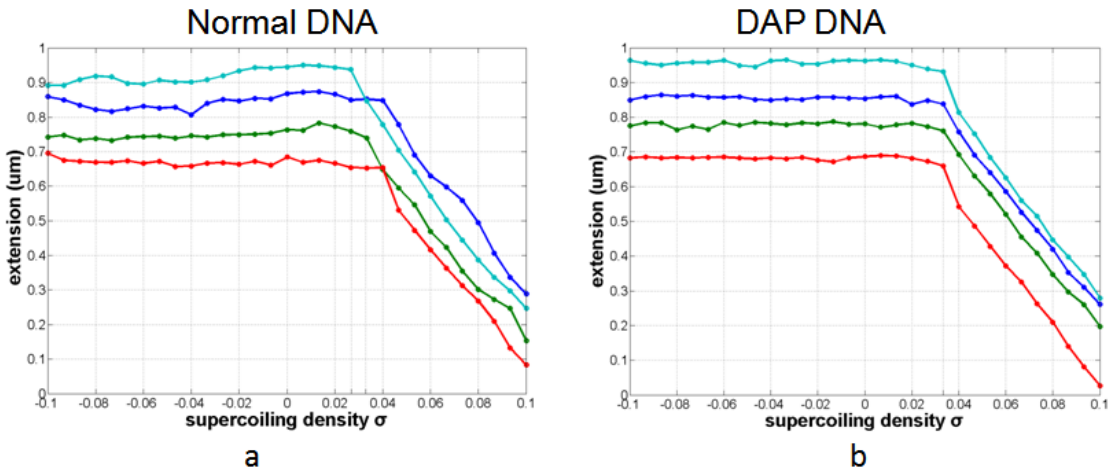

Figure 3.3 Buckling transition for normal DNA (a) and DAP DNA (b) at 1 pN. Different colors denote different DNA molecules, and extension offsets are applied on each molecule to better visualize their behavior.

However, the buckling transition point, the number of turns (N) or supercoiling density (σ) at which the DNA molecules starts supercoiling, is similar for normal and DAP DNA (N=9.4±1.3 turns and σ =0.031±0.004 for normal DNA; N= 9.7±1.4 turns and σ = 0.032±0.005 for DAP DNA). This critical number of turns, or σ, reflects the twist density that DNA can sustain, because once supercoils start to form, the twist density will be constant

over the whole DNA molecule. This result indicates that the DAP substitution hardly affects maximum twist density can be applied to DNA at a given force.

The reason why DAP incorporation stiffens DNA molecules can be explained as follows. First, DAP substitution may increase base pair stacking interaction. The extra exocyclic amino group in DAP contributes extra lone pair electrons to base pair stacking interaction increasing the stability of DNA against deformation by the external stress, such as tension and torsion. Second, DAP substitution narrows the width of the minor groove because of the presence of the extra exocyclic amino group [45, 87]. Third, the extra hydrogen bonds with thymine affect the range of twist available to base pairs [45].

§4.4 Effect of H bonds on the transition from right-handed to left-handed dsDNA

§4.4.1 DNA structural transition under high tension and extensive unwinding

When force is higher than 1 pN, because of the right handedness of DNA, the hat curves (force vs. extension) become asymmetric as shown in figure 4.4, the negative supercoiling part of the curve becomes flatter than that of the positive supercoils and the symmetric look of the curve is lost. At high forces, the unwound DNA extension remains constant. This behavior is not yet well understood. Theoreticians always avoid modeling this DNA behavior due to its mechanical complexity. The most commonly accepted explanation is that the untwisting at high force promotes local DNA denaturation at AT rich regions, therefore, instead of forming negative supercoils as it occurs at low forces (0.2 pN), DNA becomes partially denatured [11] leaving its extension unchanged. However, this denaturation hypothesis was proposed based on the indirect homologous pairing experiments performed by

Strick et al. [11]. Most of the previous experiments were performed on much longer DNA (12.5 μm) with relatively less percentage of unwinding applied on the DNA molecule (σ < 30%). Therefore I characterized the behavior of DNA at higher levels of unwinding to specifically ask the question: what kinds of deformations DNA molecules experienced during this process?

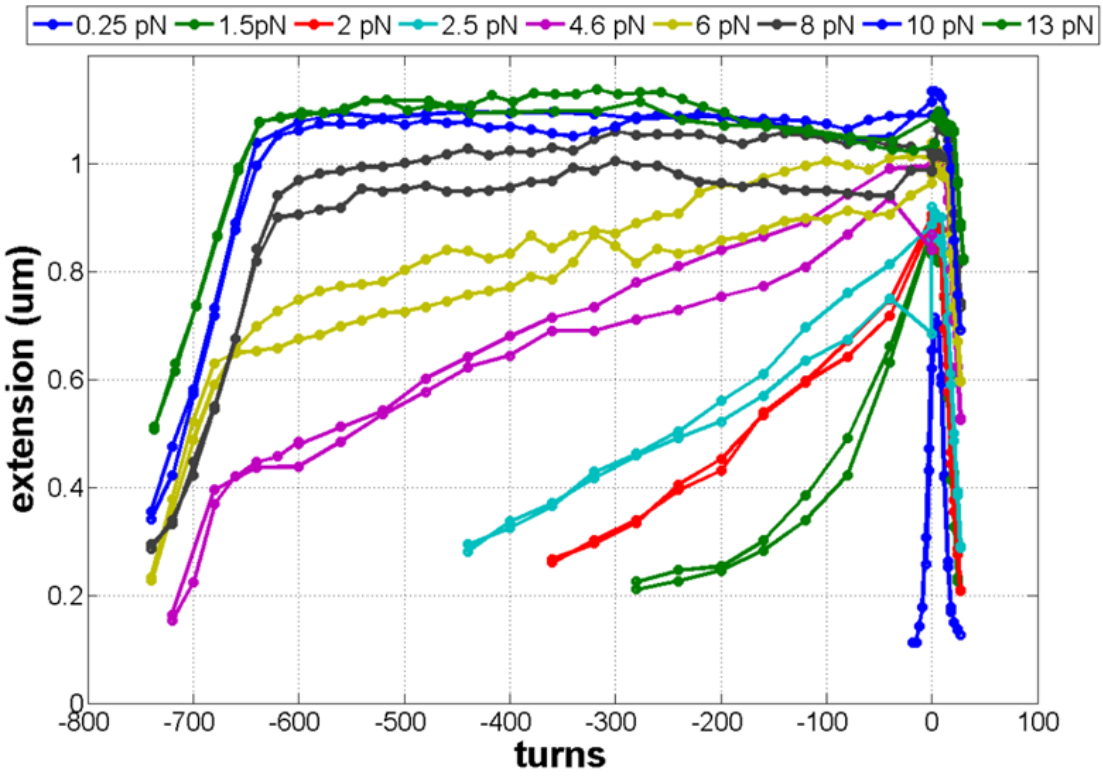

Figure 4.4 Extension vs. rotation turns data at different force for a single DNA molecule. Different colors indicate different forces.

Figure 4.4 shows the behaviors of normal DNA unwound by more than 200% from 1.5 pN to 13 pN. The percentage of unwinding is defined as supercoiling density, $\sigma = \frac{Lk - Lk_0}{Lk_0}$, Lk_0

is the linking number on torsionally unconstrained DNA which can be calculated using the total number of base pairs divided by 10.4 bp/turn in B-DNA, for example for our 3200 bp DNA, Lk_0=308 turns. Lk-Lk_0 is the change in linking number due to the externally applied torsion. In our case, Lk-Lk_0 equals to the number of turns being applied to the single DNA molecules. Therefore more than -600 turns correspondent to -200% degrees of supercoilings. The symmetric hat curve at 0.25 pN served as the control to ensure the DNA behaves normally at low force. At forces from 1.5 pN to 2.5 pN, DNA extension still decreases linearly with increasing number of negative turns with the slope smaller than that observed for positive turns. However, if we interpret the change in extension due to the formation of negative plectonemes, the estimated size of a plectonemic loop from the slope of the linear region of this curve is less than 2 nm for this force range. This is smaller than the helical pitch of dsDNA, thus this size is not realistic. Therefore, there must be either a mixture of supercoiling (extension decrease) and denaturation (extension increase) or conformation transition (mild length decrease). Increasing the force from 4.6 pN to 13 pN, the extension decrease becomes less and less significant till at the 8 pN DNA extension remain unchanged even at -200% degrees of supercoiling. In this force range, the unwinding of DNA promotes the transition from right handed B-form to left handed conformation [32]. At around -200%, DNA is converted fully to left handed helical structure (L-DNA) with the similar pitch as in B-DNA, because linking number changes from 308 turns to almost -308 turns. The significant extension drop observed at $\sigma < -200\%$ indicates that the L-DNA forms plectoneme upon further unwinding. L-DNA always supercoils beyond $\sigma < -200\%$, which indicates that DNA has already completely turned into L-DNA, thus any further unwinding contributes only to plectoneme formation not to phase transition.

§4.4.2 Effect of H bonds on right hand to left hand transition

Investigating the effect H bonds on right hand to left hand transition is very important to understand the type of deformation that DNA undergoes during the transition, for example, denaturation is sensitive to the GC percentage of the DNA [11] and GC repeat are more easier to transit to left handed Z-DNA form [14]. Recently, a model for a left double helical structure with all the base pairing disrupted was proposed by Sheinin from Michelle Wang's group [88] for unwound DNA at high tension, the same condition studied in this chapter. Therefore, the higher the GC percentage (more H bonds), the easier it should be to observe a sequence effect. Synthesizing 100% GC (all triple H bonds) DNA up to 3000 bp is impractical given the available DNA synthesis techniques, such as PCR or chemical synthesis. Therefore, we use the DAP DNA as the model system to investigate how H bonds affect the right hand to left hand transition.

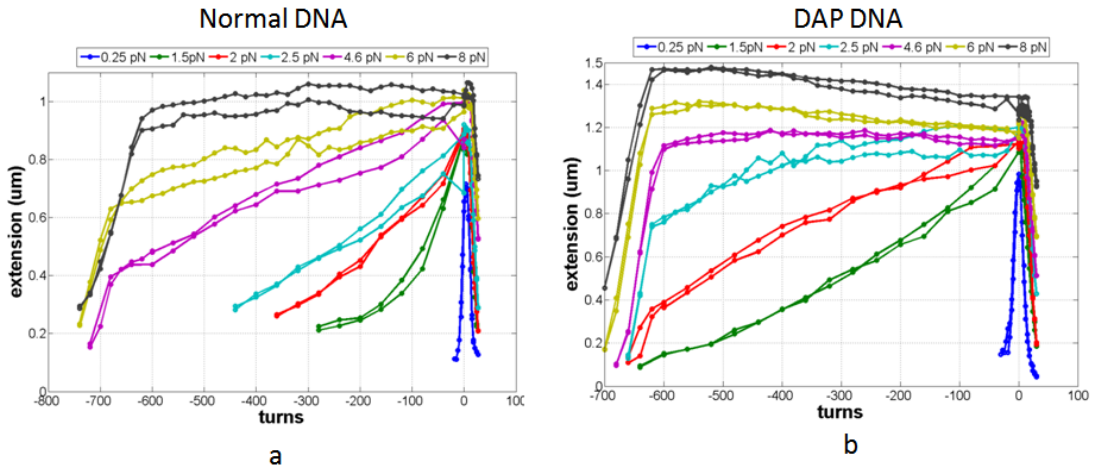

Figure 4.5 Underwound single normal DNA (a) and DAP DNA (b) molecule at high force. The same color indicates the same force.

Figure 4.5 displays the behavior of normal and DAP DNA unwound at forces from 1.5 pN to 8 pN. The hat curves at 0.25 pN serve as control for both cases. One of the most significant differences between the two types of molecules is that DAP DNA shortens less than normal DNA at the same tension during unwinding. The other difference is that DAP DNA seems to change to the left handed structure at lower force compared to normal DNA. Therefore, the data reveal that the right hand to left hand transition is highly H bonding dependent. Also, on one hand, recall that GC bps do not denature as easily as AT bps, similarly, DAP DNA should be more difficult to denature. However, this is not my hat curves showed. I conclude that unwound DNA must experience a conformational change that is more complicated than only denaturation. On the other hand, the transition from B-DNA to left handed Z-DNA occurs more easily in DNA with GC sequence repeats [14]. Therefore, DAP DNA is more prone to convert to left handed DNA than normal DNA, which agrees with what I observed. However, whether the left handed DNA stabilized by the negative torsion is Z- DNA or DNA without base pairing is not yet clear. In addition, comparing to the flat region of the curves before L-DNA buckles from 0 to -600 turns at 8 pN, the extension of DAP DNA mildly increases while normal DNA remain the same, which indicates the DAP DNA is easier to be overstretched. This behavior agrees well with the experiments state that increasing GC% promote DNA transition to over-stretching dsDNA [89].

§4.4.3 Dynamics of left hand to right hand transition

The experimental procedure to obtain the force vs. extension curves shown in figure 4.4 and 4.5 is as follows. Extension data were taken during unwinding of the DNA to several hundred turns and winding it back to the torsional unconstrained state every 20 turns. This procedure yielded two curves at the same force in figure 4.3. The hysteresis in those pairs of curves is

pronounced when the force values are in the range from 2.5 pN to 8 pN for normal DNA. The DNA extension is always lower when the molecule is being wound back than when it is unwound. These results indicate that the right to left hand and left to right hand transition are not following the same path. Especially, if one looks closely to the extension at 0 turns, at 2.5 pN and 4.6 pN, when DNA is wound back, this value is much less than the DNA extension in the torsionally relaxed state. However, it only takes less than one minute for the DNA to recover from the low extension to its original extension. Every data point in the extension vs. turns curve is the time average over 100 images of the extension in the same condition, therefore, this recovery transition contributes to the lower average of the extension value.

In order to gain a better understanding of the transition from left to right-handed helix, I monitored the extension at 2.5 pN in real time during unwinding and rewinding of normal DNA molecules (Fig. 4.6). In figure 4.6a, DNA was unwound to -600 turns (σ = -200%), let stand for several minutes and then rewound back to 0 turns at a rate of 15 turns per second. The arrows indicate the data taken while the magnet was rotating. The DNA extension decreases smoothly when unwound to -600 turns. However, the extension increases smoothly at first when rewound to 0 turn, and drops significantly during the very last few turns. This low extension state is not stable and quickly changes to the original extension at 0 turns in three steps (circled in figure 4.6a). Measurements were conducted by unwinding DNA to -300 turns and rewinding back. Similar curves were observed, even if the extension drops were smaller than those observed in the -600 case. The recovery also happened in three steps. This similarity between these two types of measurements indicates the same type of conformational rearrangement. However, I was unable to observe this rearrangement when unwinding and rewinding DNA to and back from -40 turns. This behavior does not occur on DAP DNA based on experimental results for DAP DNA.

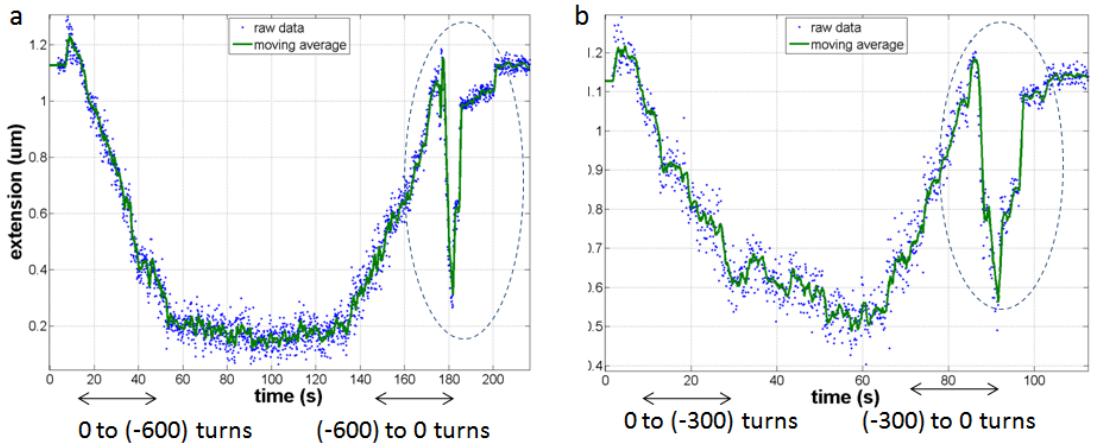

Figure 4.6 Dynamic traces of left hand to right hand transition. From -600 turns (a) and -300 turns (b) at 2.5 pN. The circled area shows the view of the three steps recovery to B-form DNA.

The data shown in figure 4.6 are from the same DNA molecule at 2.5 pN. Therefore, in order to thoroughly investigate this recovery behavior we need to collect more data from different DNA molecules as well as at various forces, degrees of unwinding and speed of magnet rotation.

This recovery behavior occurring for normal DNA not DAP DNA seems to indicate the number of H bonding dependence, specifically the different deformation of AT or GC rich region. A simple explanation for this extension drop and recovery could be the following in figure 4.7. When being rewound before the last few tenth number of turns, most part of DNA should already be in B-form perhaps with a small percentage of denaturation or left handed structure (figure 4.7a), thus the last few tenth of turns rewinding induced the positive supercoiling formation in the B-DNA portion leaving the local deformation untouched (figure

4.7b). Finally, DNA will rearrange this energetically unfavorable state to the state with homogenouse B-form along the contour of DNA molecule in two steps (figure 4.7c).

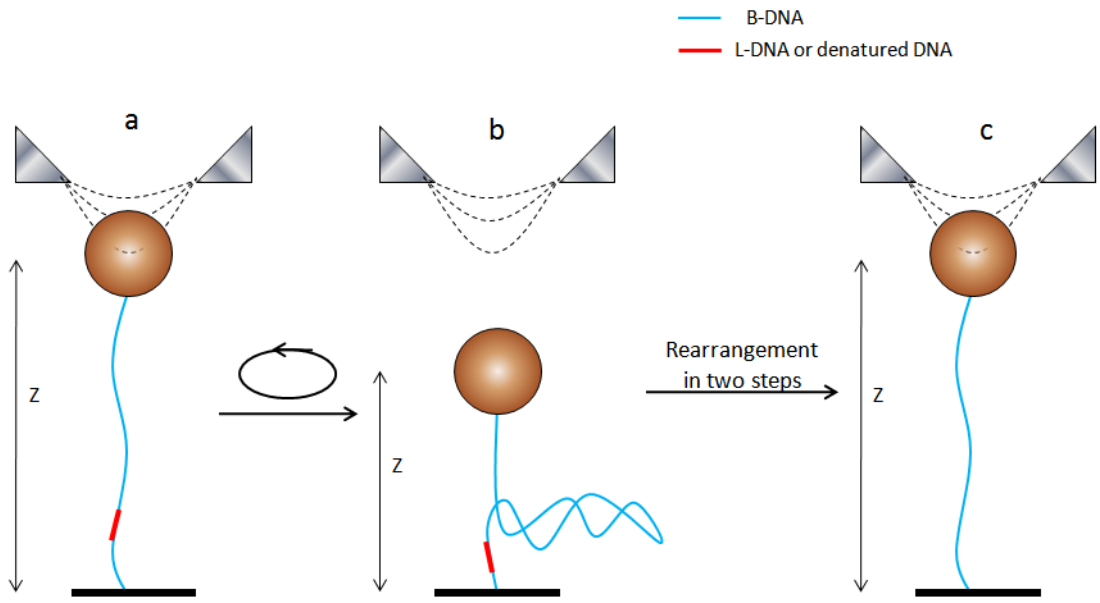

Figure 4.7 Schematic illustration of DNA extension drop and recovery during rewinding. The drawing is not to scale.

The plateaus between the recovery steps represent two intermediate or transition states with different stability. This stepwise trace indicates more than one types of conformation rearrangement happens during the process.

Chapter 5

DNA stiffness affects Type II topoisomerases - DNA interaction and activity

§5.1 Outline

In this chapter, I investigated how DNA stiffness affects type II toposiomerases activity. The stiffer DAP DNA molecule was used as a substrate to compare with normal DNA. Two kinds of type II topoismerases were used in this study, *E coli.* gyrase and recombinant human topoII alpha. In the first part of this chapter. EMSA and Magnetic Tweezers experiments to investigate how DAP DNA affects the binding affinity and wrapping ability of gyrase ae described. In the second part, the rates and processivity of supercoiling relaxation by gyrase and recombinant human topoII on normal and DAP DNA are described.

§5.2 DAP DNA affects the binding of *E. coli* Gyrase to DNA

§5.2.1 The binding affinity of *E. coli* gyrase was reduced on DAP DNA

One of the most widely used techniques for investigating the ability of proteins to bind DNA is an Electrophoretic Mobility Shift Assay (EMSA). The binding affinity can be determined by comparing the percentages of free and protein bound DNA at different protein concentrations. The representative gels shown in figure 5.1a reveal gyrase binding to normal and DAP DNA. The intensities of the free and protein-bound DNA bands reflect the equilibrium between equal amounts of DNA (1 pmol in 25 μl of reaction buffer) but increasing gyrase concentrations as indicated in the figure. As the concentration of gyrase increased, the free DNA band becomes less intense (lower band), while protein bound DNA bands become more intense (higher band). These intensity changes (band shifts) reflect the binding affinity of gyrase to DNA. Comparing to the gels reveals that although the percentage of gyrase binding on DAP DNA still increased with increasing gyrase concentrations, more gyrase was bound to normal DNA at the same concentrations.

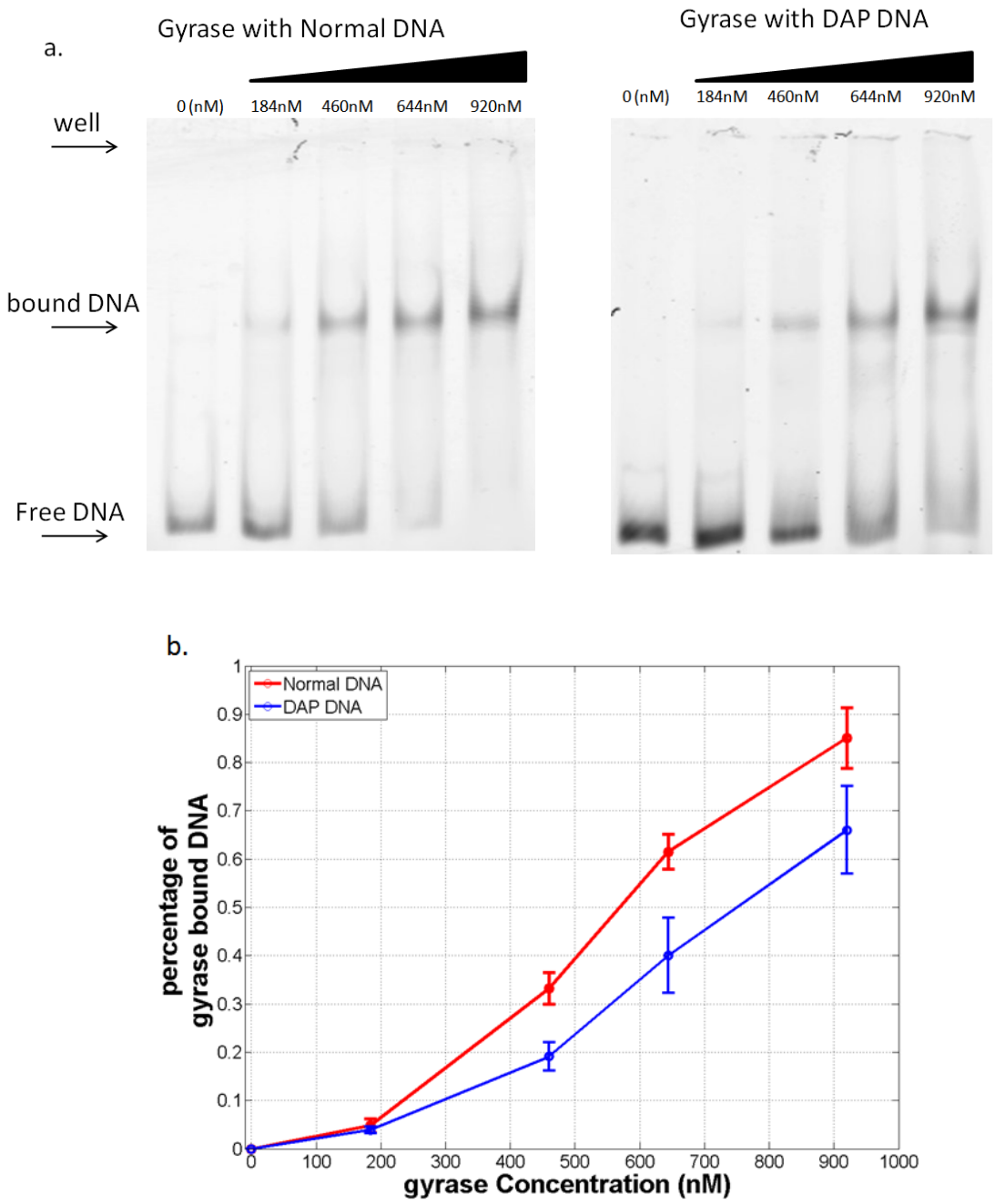

Figure 5.1 EMSA of gyrase binding to normal and DAP DNA. (a) representative gels to assay binding with increasing gyrase concentration on normal and DAP DNA. (b) average percentages of gyrase bound -DNA at different gyrase concentrations for normal and DAP DNA.

Therefore, this result reveals that gyrase has reduced binding affinity for DAP DNA. The percentage of protein-complexed DNA band was quantified by densitometry analysis. Figure 5.1b shows the average percentage vs. gyrase concentration data for five EMSA experiments for normal and DAP DNA. The binding affinity of gyrase was reduced by about 20% for DAP DNA for the gyrase concentrations higher than 184 nM. This quantitatively analysis showed that the stiffness of DNA affects the binding affinity of gyrase, and suggests that there is a significant conformational change, such as bending or wrapping of DNA, associated with gyrase binding.

§5.2.2 The wrapping ability of *E. coli* gyrase was reduced for DAP DNA

E. coli. gyrase has been used to investigate how the physical properties of DNA, especially the stiffness, affect the function of enzymes. Gyrase is known to nonspecifically wrap DNA fragment up to 180 degrees around the C-terminal domain [4]. This wrapping process is believed to facilitate introducing negative supercoils and relaxing positive supercoils of DNA in the presence of ATP [90]. However, researchers have found that without ATP gyrase can still wrap DNA at low tension. Without energy consuming, the DNA wrapping is reversible: there is an unwrapping and wrapping equilibrium [91]. Therefore in order to investigate the wrapping ability of gyrase on stiffer DAP-substituted DNA comparing to normal DNA, I conducted the experiments at 0.4 pN without ATP on torsionally relaxed DNA. Before adding gyrase into the chamber, control measurements were conducted to verify that transitions between wrapped (shortened) and unwrapped states were due to gyrase. After adding the gyrase into the chamber, data were recorded for hours.

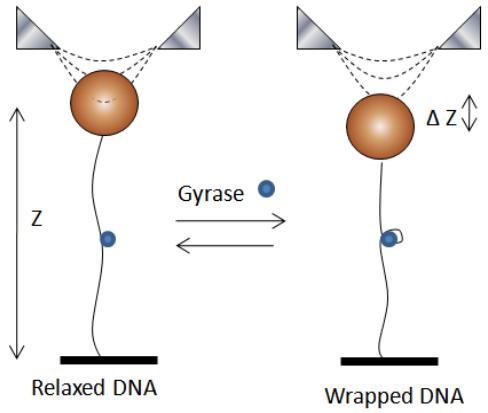

Figure 5.2 Schematic illustration of gyrase wrapping detected with Magnetic Tweezers. The drawing is not to scale.

The representative traces show that gyrase wrapped DAP-substituted DNA much less frequently than normal DNA (Fig 5.3a, b). All the wrapping traces were analyzed using 10 s time filter to suppress the noise due to the thermal fluctuation of the bead. The cumulative histograms of DNA extension in Fig 5.3c and d show two distinct peaks for both normal and DAP-substituted DNA experiments. The separation between these two peaks is about 35 nm for both cases which is consistent with the length of DNA wrapped by the C-terminal domain of gyrase reported in other studies [4]. The relative proportions of areas under the two peaks revealed that the probability for gyrase to wrap DAP-substituted DNA is distinctly lower than that of normal DNA. Employing a Boltzmann distribution, the free energy required to wrap DNA was estimated using these proportions. The energy required for gyrase to wrap DAP-substituted DNA is 5.9 kJ/mole compared to 4.0 kJ/mol for normal DNA. These energy differences might result from the fact that DAP-substituted DNA is stiffer and requires more energy to bend. From the structural and electrostatic study of C-terminal domain of gyrase,

Corbett proposed that gyrase bends DNA in a series of three 60 degree kinks to produce a total 180 degree arc [4] .

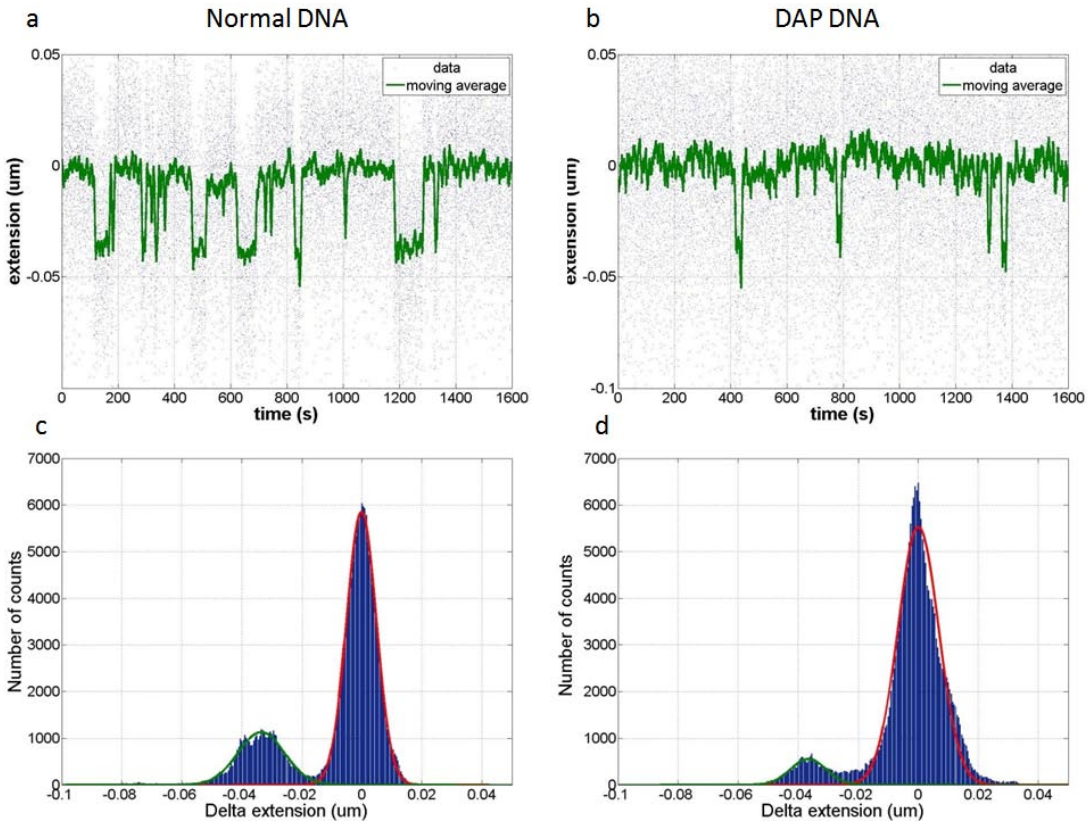

Figure 5.3 Gyrase wrapping assay on normal and DAP DNA. The top panel is a representative gyrase wrapping record on normal (a) and DAP (b) DNA. Raw data are plotted in dots, and the solid lines are moving averages with a time window of about 10 seconds. Since gyrase wrapping is reversible in the absence of ATP, the extension of the DNA alternates between two levels, the high level represents the unwrapped state while the low one represents the wrapped state. The bottom panel is the cumulative histogram of the lengths of normal (c) and DAP (d) DNA incubated with gyrase. The histogram was fitted with two Gaussian curves representing the unwrapped (high peak) and wrapped state (low peak) respectively.

Model building studies revealed that the DNA double helix is most easily kinked by flexion toward the minor groove, the existence of exocyclic amino groups in the minor grove of DAP-substituted DNA limit the narrowing of the minor grove, therefore kinking of DAP-substituted DNA requires more energy [87]. Recent energy measurements of nucleosome affinity to normal and DAP-substituted fragments reveal the free energy difference is about 3.8 kJ/mole which is comparable to our data which is 2 kJ/mole [45].

§5.3 The activity of *E. Coli* gyrase on supercoiled DAP and normal DNA

In addition to wrapping DNA by 180 degrees , gyrase, may bend DNA up to 150 degrees like the yeast type II topoisomerase [18]. Since this bending likely happens once every enzymatic cycle the activity of gyrase might be faster on normal with respect to DAP-substituted DNA. Therefore, gyrase activity was measured to determine whether DNA bending is rate limiting step of the enzymatic cycle. Hat curves for each DNA molecule were recorded before adding enzymes. By calculating the slope of the positive, linear part of the hat curves, the changes of DNA extension were correlated to numbers of supercoils. Then buffer containing gyrase and ATP was added into the flow chamber. After waiting for several minutes, DNA under 0.6 pN tension was twisted 30 turns, equivalent to about 10% supercoiling density for DNA with a length of about 3000 bps. Three representative relaxation curves from different DNA molecules at 1 mM ATP concentration are shown in figure 5.5a and b. The shape of the curves showed that relaxation of supercoiling happens in steps. Two features of the relaxation traces were analyzed: one was the slope of the bursts of relaxation, defined as the relaxation rate which represents the activity of the enzyme if the unit is converted from nm/s to turns/s,

the conversion factor can be obtained from extension vs. turns curves at the same force; the other was the interval between two consecutive bursts, defined as a pause.

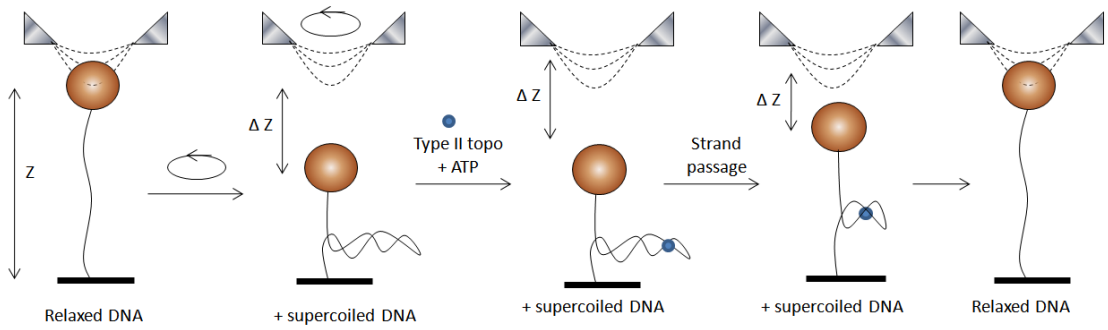

Figure 5.4 Schematic illustration of enzyme-catalyzed supercoil relaxation monitored using Magnetic Tweezers. The drawing is not to scale.

The relaxation curves were recorded for both normal and DAP-substituted DNA at different ATP concentrations: 0.1 mM, 0.2 mM, 0.5 mM, 1 mM and 1.5 mM. . The results in figure 5.5c showed that the overall rate decreased with DAP-substituted DNA substrate when the ATP concentration was near or above a saturating level. Previous studies of the relaxation DNA supercoils by *E. coli* gyrase using Magnetic Tweezers technique have shown that the rate of gyrase-catalyzed relaxation of positive supercoils reaches the maximum value of 2.2 turns/s around 0.6 pN at 1 mM ATP concentration [90]. The present data revealed a very similar rate of around 2.2 turns/s under these conditions for normal DNA in our experiments.

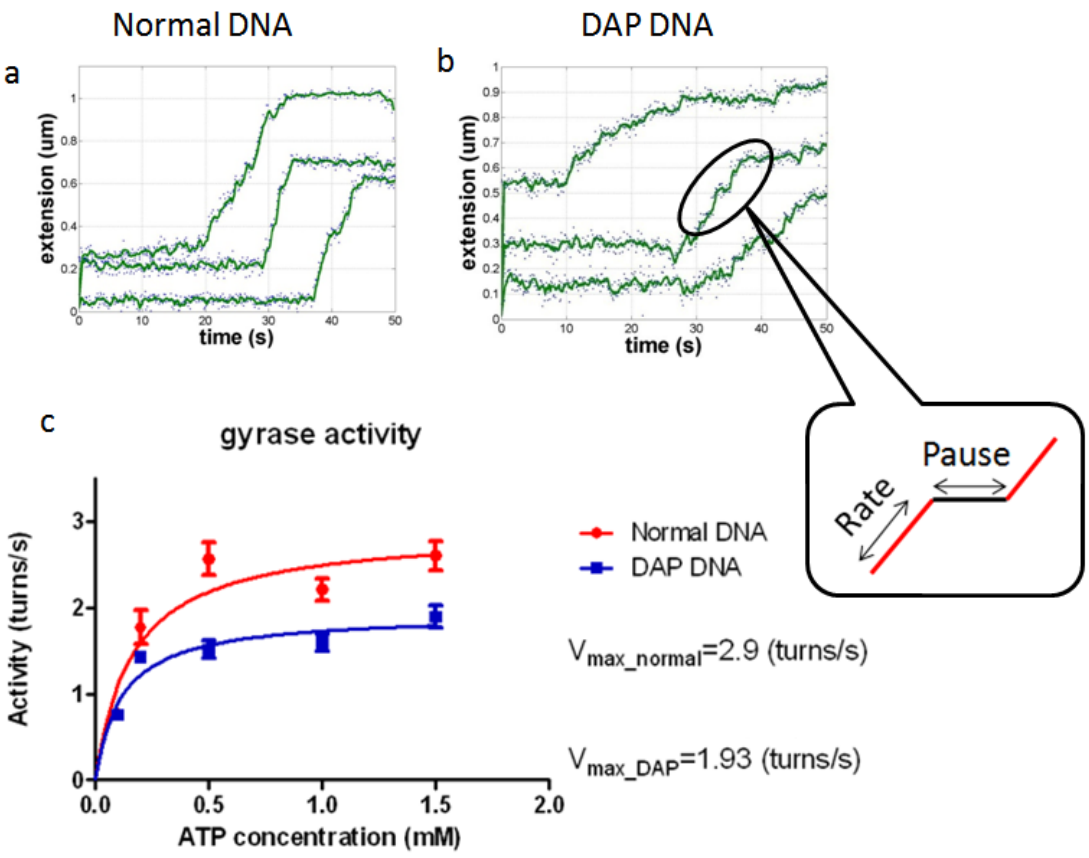

Figure 5.5 Activity of gyrase on normal and DAP DNA. Representative records of gyrase-catalyzed relaxation on normal (a) and DAP DNA (b) at 1 mM ATP and 0.6 pN tension. The dots are raw data, the solid line are moving averages over 5 raw data points. (c). The activity of gyrase at different ATP concentrations on normal (red) and DAP (blue) DNA. The solid lines are Michaelis-Menten fittings.

The activity vs. ATP concentration data was fitted using the Michaelis-Menten model in equation 5.1:

$$V_0 = \frac{V_{\max}[ATP]}{K_M + [ATP]} \qquad \textbf{[Eq.5.1]}$$

Fitting established a V_{max} of 2.9 turns/s for normal DNA, while for DAP-DNA V_{max} was only 1.93 (turns/s). The DAP substrate slowed down gyrase by one third of the original rate, suggesting that DNA stiffness affects the activity of gyrase. The simplest explanation that is consistent with other studies is that gyrase must bend the "gate" DNA segment to relax supercoils.

Between consecutive bursts of supercoil relaxation there were some pauses during which, gyrase may remain in contact with the DNA molecule waiting for ATP or switching to an active conformation for the next enzymatic cycle. Another possibility is that one gyrase molecule may detach from the DNA until the same or a different gyrase molecule binds DNA to continue the relaxation process. Since the distribution of truly paused, but not detached enzymes can reveal characteristic rate limiting steps of the enzymatic cycle, pauses corresponding to gyrase still associated with DNA were measured. In order to exclude pauses due to unbinding and rebinding events, the average time lag between mechanically introducing supercoiling and the start of supercoil relaxation by gyrase was noted. This time interval represented the time spent by the enzyme searching for supercoiled DNA substrate. All pauses longer than about 100s, the mean searching time, which was very similar for normal and DAP DNA, were excluded.

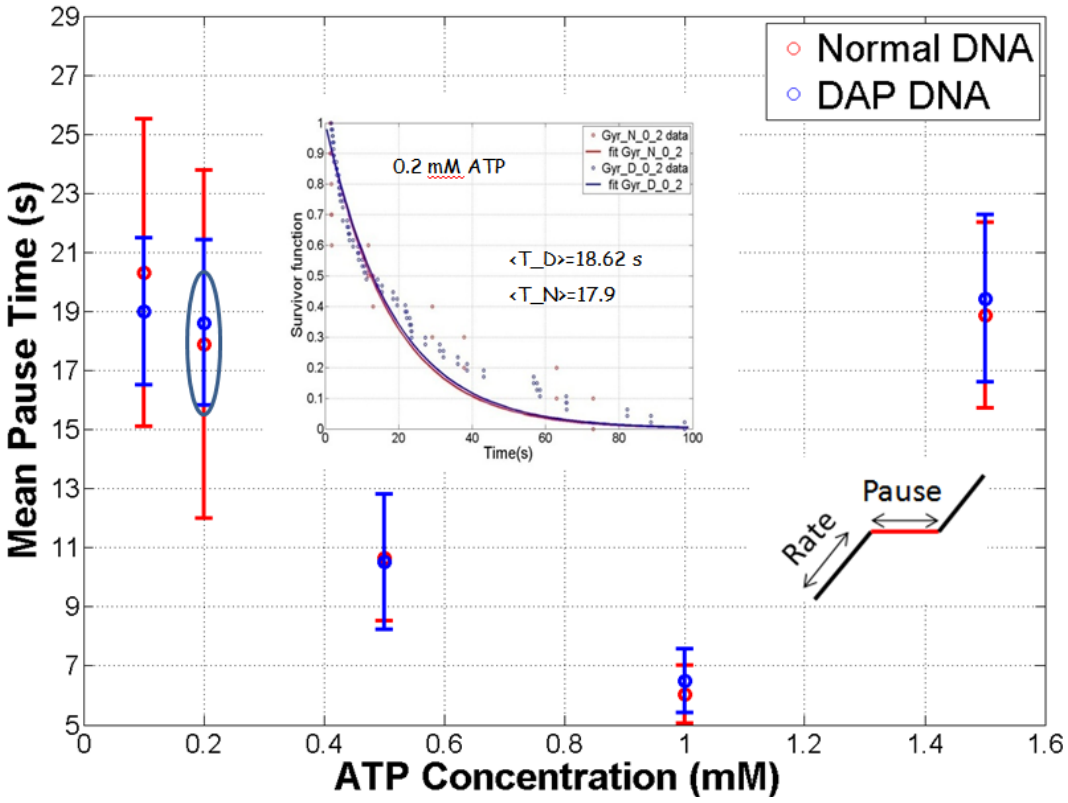

Figure 5.6 Mean pause time of gyrase at different ATP concentrations for normal and DAP DNA. Red is normal DNA and blue is DAP DNA. The mean pause times were determined by fitting pause distributions using single exponentials for each ATP concentration on normal and DAP DNA respectively. The inset is an example fitting of the pause distribution at 0.2 mM ATP.

During all the remaining pauses gyrase was assumed to be associated with the DNA tether. Survival functions of the pause distributions for DAP DNA almost overlapped with those of normal DNA. Fitting with single–exponential decays established similar mean decay

constants for both types of DNA, which decreased with increasing ATP concentration except at 1.5 mM ATP concentration. Thus ATP appears to bind during pauses and the stiffness of DNA did not affect the pause distribution. These results imply that DNA bending is not a rate-limiting step for the initiation of a strand passage event by gyrase. Recent affinity assays have shown that a unique domain insertion in gyrase is crucial for DNA-binding, and removal of this insertion reduced the binding affinity significantly [79]. This insertion could enable gyrase to bind without deforming DNA during a pause. The poor fitting by single exponentials suggests more than one rate limiting step comprising multiple paused states between enzymatic cycles. Indeed, gyrase molecules may delay as they shift between relaxation modes with and without wrapping [90].

§5.4 The activity of recombinant human topoII alpha on supercoiled DAP and normal DNA

To better understand how DNA stiffness affects type II topoisomerase activity, identical assays were performed using human topoisomerase II alpha. Similarly to gyrase, human topoisomerase II alpha employs a two-gate mode of strand passage; however, unlike gyrase, the C-terminal domain of human topoisomerase II alpha does not wrap DNA around itself to facilitate the capture of the transfer segment during an enzymatic cycle [92]. This structure difference excluded the wrapping mode of positive supercoil relaxation for human topoII alpha. The same experimental conditions adopted for gyrase were used for this assay. Figure 5.7a and b show representative relaxation traces for three different DNA molecules for normal and DAP-substituted DNA respectively.

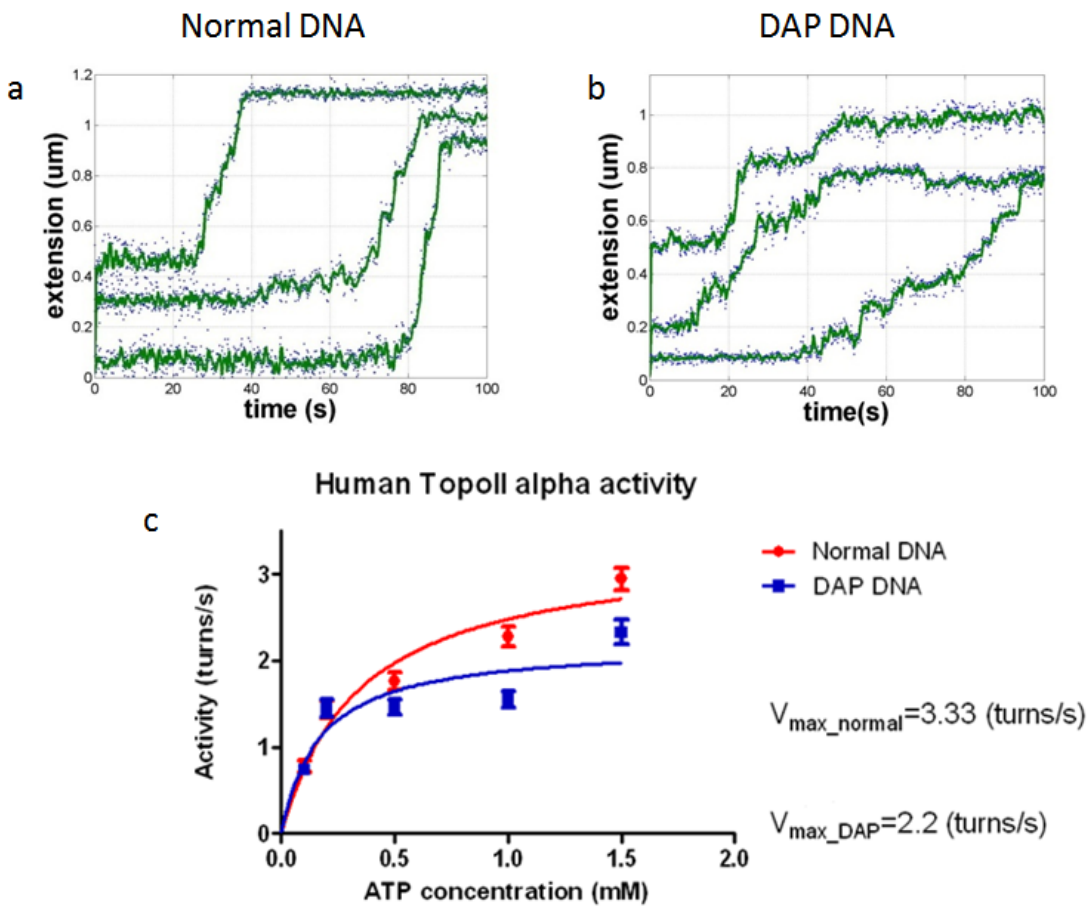

Figure 5.7: Activity of human topoisomerase II alpha on normal and DAP DNA Representative relaxation traces by human topoII on normal (a) and DAP DNA (b) at 1 mM ATP and 0.6 pN. The dots are raw data, the solid line are moving averages of 5 raw data points. (c) The activity of human topoII alpha at different ATP concentrations on normal (red) and DAP (blue) DNA. The solid lines are Michaelis-Menten fitting for normal and DAP DNA respectively.

As for gyrase, the overall rate of supercoil relaxation decreased with the DAP-substituted substrate when the ATP concentration was near or above the saturated level (figure 5.7 c).

Fitting both normal and DAP data using Michaelis-Menten models established a V_{max} of 3.3 turns/s for normal DNA, while for DAP DNA V_{max} was 2.2 (turns/s). Thus the DAP substrate also slowed down the human topoII alpha by one third of the original rate for normal DNA and strongly suggests that human topoII alpha also bends DNA during the strand passage reaction.

To analyze the pauses, pauses greater than or equal to the mean searching time (see section 5.3) were assumed to derive from enzyme dissociation and reassociation with the DNA and were discarded. Similar to gyrase data, the decay constants from fitting for both DAP and normal DNA decrease with increasing ATP concentration. Unlike gyrase data, the survival functions of pause distributions were satisfactorily fitted by single exponentials. Furthermore the pause distributions for DAP DNA were significantly different from those of normal DNA, and the decay constants were larger. These results indicated that rate limiting steps that changed the duration of the pauses were affected by the stiffness of DNA molecule. Similar to what was found for gyrase, the ATP dependence of pauses also indicated ATP binding during the pauses. As for gyrase, the stiffness of DNA modified the activity of human topoII alpha, strongly suggesting that it also bends DNA. The lack of an insertion in human topoII alpha such as that of gyrase, which increases its affinity for DNA, might allow gyrase to more readily bind and bend DNA and begin a cycle of strand passage [79].

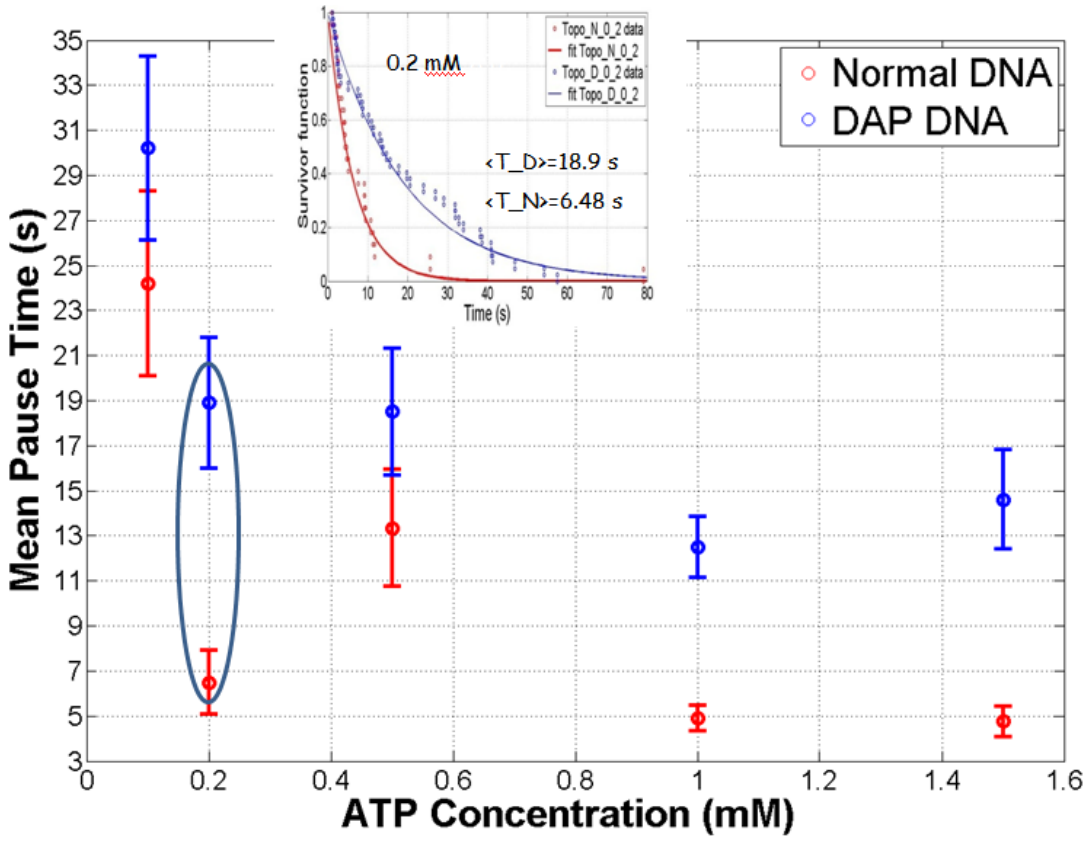

Figure 5.8 Mean pause times of human topoII alpha at different ATP concentrations for normal and DAP DNA. Red is normal DNA and blue is DAP DNA. The mean pause times were acquired by fitting pause distributions using single exponentials at each ATP concentration for normal and DAP DNA respectively. The inset is the fitting of the pause distribution for 0.2 mM ATP.

§5.6 Conclusion

Using single molecule Magnetic Tweezers, the persistence length of the DAP-substituted DNA reflected increased stiffness through increased base pair stacking and H bonding of DNA. The ability of the C-terminal domain of gyrase to wrap stiffer DNA decreased, which is consistent with the dependence of DNA deformation on the percentage of triple H bonded GC base pairs. The decreases of the overall supercoil relaxation rates of both gyrase and

recombinant human topoII alpha indicate that bending occurs in the rate limiting steps of their enzymatic cycles, which are therefore affected by the stiffness of DNA. The discrepancies of the effects of DNA stiffness on the pause distributions of gyrase and recombinant human topoII alpha reflect different binding modes due to the structural differences of those two enzymes.

References

1. Nakabachi, A., et al., *The 160-kilobase genome of the bacterial endosymbiont Carsonella.* Science, 2006. **314**(5797): p. 267-267.
2. Pellicer, J., M.F. Fay, and I.J. Leitch, *The largest eukaryotic genome of them all?* Botanical Journal of the Linnean Society, 2010. **164**(1): p. 10-15.
3. Finzi, L. and J. Gelles, *Measurement of lactose repressor-mediated loop formation and breakdown in single DNA molecules.* Science, 1995. **267**(5196): p. 378-80.
4. Corbett, K.D., R.K. Shultzaberger, and J.M. Berger, *The C-terminal domain of DNA gyrase A adopts a DNA-bending beta-pinwheel fold.* Proc Natl Acad Sci U S A, 2004. **101**(19): p. 7293-8.
5. Rice, P.A., et al., *Crystal structure of an IHF-DNA complex: a protein-induced DNA U-turn.* Cell, 1996. **87**(7): p. 1295-306.
6. Kusano, T., et al., *Polyamines: essential factors for growth and survival.* Planta, 2008. **228**(3): p. 367-381.
7. Wallace, H.M., A.V. Fraser, and A. Hughes, *A perspective of polyamine metabolism.* Biochemical Journal, 2003. **376**: p. 1-14.
8. Watson, J.D. and F.H.C. Crick, *Molecular Structure of Nucleic Acids - a Structure for Deoxyribose Nucleic Acid.* Nature, 1953. **171**(4356): p. 737-738.
9. Garrett, H.R.a.G., C. M., *Biochemistry*. 2005: David Harris
10. Dove, W.F. and N. Davidson, *Cation Effects on Denaturation of DNA.* Journal of Molecular Biology, 1962. **5**(5): p. 467-&.
11. Strick, T.R., V. Croquette, and D. Bensimon, *Homologous pairing in stretched supercoiled DNA.* Proceedings of the National Academy of Sciences of the United States of America, 1998. **95**(18): p. 10579-10583.
12. Ouameur, A.A. and H.A. Tajmir-Riahi, *Structural analysis of DNA interactions with biogenic polyamines and cobalt(III) hexamine studied by Fourier transform infrared and capillary electrophoresis.* Journal of Biological Chemistry, 2004. **279**(40): p. 42041-42054.
13. Jones, S., et al., *Protein-DNA interactions: A structural analysis.* Journal of Molecular Biology, 1999. **287**(5): p. 877-896.
14. Dickerson, R.E., et al., *The Anatomy of a-DNA, B-DNA, and Z-DNA.* Science, 1982. **216**(4545): p. 475-485.
15. Pohl, F.M. and T.M. Jovin, *Salt-Induced Cooperative Conformational Change of a Synthetic DNA - Equilibrium and Kinetic Studies with Poly(Dg-Dc).* Journal of Molecular Biology, 1972. **67**(3): p. 375-&.
16. Pohl, F.M., *Polymorphism of a Synthetic DNA in Solution.* Nature, 1976. **260**(5549): p. 365-366.
17. Lee, M., S.H. Kim, and S.C. Hong, *Minute negative superhelicity is sufficient to induce the B-Z transition in the presence of low tension.* Proceedings of the National Academy of Sciences of the United States of America, 2010. **107**(11): p. 4985-4990.
18. Dong, K.C. and J.M. Berger, *Structural basis for gate-DNA recognition and bending by type IIA topoisomerases.* Nature, 2007. **450**(7173): p. 1201-U4.
19. Wang, M.D., et al., *Force and velocity measured for single molecules of RNA polymerase.* Science, 1998. **282**(5390): p. 902-907.

20. Bockelmann, U., et al., *Unzipping DNA with optical tweezers: high sequence sensitivity and force flips.* Biophysical Journal, 2002. **82**(3): p. 1537-1553.
21. Smith, D.E., et al., *The bacteriophage phi 29 portal motor can package DNA against a large internal force.* Nature, 2001. **413**(6857): p. 748-752.
22. Simmons, R.M., et al., *Quantitative measurements of force and displacement using an optical trap.* Biophysical Journal, 1996. **70**(4): p. 1813-1822.
23. Strick, T.R., et al., *The elasticity of a single supercoiled DNA molecule.* Science, 1996. **271**(5257): p. 1835-1837.
24. Florin, E.L., V.T. Moy, and H.E. Gaub, *Adhesion Forces between Individual Ligand-Receptor Pairs.* Science, 1994. **264**(5157): p. 415-417.
25. Marko, J.F. and E.D. Siggia, *Stretching DNA.* Macromolecules, 1995. **28**(26): p. 8759-8770.
26. Bednar, J., et al., *Determination of DNA Persistence Length by Cryoelectron Microscopy - Separation of the Static and Dynamic Contributions to the Apparent Persistence Length of DNA.* Journal of Molecular Biology, 1995. **254**(4): p. 579-591.
27. Forth, S., et al., *Abrupt buckling transition observed during the plectoneme formation of individual DNA molecules.* Physical Review Letters, 2008. **100**(14): p. -.
28. Purohit, P.K., *Shape and energetics of DNA plectonemes*, in *IUTAM symposium on Cell, Molecular and Tissue* 2010.
29. Clauvelin, N., B. Audoly, and S. Neukirch, *Elasticity and Electrostatics of Plectonemic DNA.* Biophysical Journal, 2009. **96**(9): p. 3716-3723.
30. Moroz, J.D. and P. Nelson, *Entropic elasticity of twist-storing polymers.* Macromolecules, 1998. **31**(18): p. 6333-6347.
31. Mosconi, F., et al., *Measurement of the Torque on a Single Stretched and Twisted DNA Using Magnetic Tweezers.* Physical Review Letters, 2009. **102**(7): p. -.
32. Sarkar, A., et al., *Structural transitions in DNA driven by external force and torque.* Physical Review E, 2001. **6305**(5): p. -.
33. Smith, S.B., Y.J. Cui, and C. Bustamante, *Overstretching B-DNA: The elastic response of individual double-stranded and single-stranded DNA molecules.* Science, 1996. **271**(5250): p. 795-799.
34. Leger, J.F., et al., *Structural transitions of a twisted and stretched DNA molecule.* Physical Review Letters, 1999. **83**(5): p. 1066-1069.
35. Cantor, C.a.S., P., *Biophyaical Chemistry part III: The behavior of Biological Macromolecules*. 1980, New York.
36. Podesta, A., et al., *Positively charged surfaces increase the flexibility of DNA.* Biophysical Journal, 2005. **89**(4): p. 2558-63.
37. Bustamante, C., et al., *Single-molecule studies of DNA mechanics.* Curr Opin Struct Biol, 2000. **10**(3): p. 279-85.
38. Okonogi, T.M., et al., *Flexibility of duplex DNA on the submicrosecond timescale.* Biophysical Journal, 1999. **77**(6): p. 3256-76.
39. Strick, T., et al., *Twisting and stretching single DNA molecules.* Prog Biophys Mol Biol, 2000. **74**(1-2): p. 115-40.
40. Peters, J.P., 3rd and L.J. Maher, *DNA curvature and flexibility in vitro and in vivo.* Q Rev Biophys, 2010. **43**(1): p. 23-63.
41. Manning, G.S., *The persistence length of DNA is reached from the persistence length of its null isomer through an internal electrostatic stretching force.* Biophysical Journal, 2006. **91**(10): p. 3607-16.

42. Baumann, C.G., et al., *Ionic effects on the elasticity of single DNA molecules.* Proc Natl Acad Sci U S A, 1997. **94**(12): p. 6185-90.
43. Hagerman, K.R. and P.J. Hagerman, *Helix rigidity of DNA: the meroduplex as an experimental paradigm.* Journal of Molecular Biology, 1996. **260**(2): p. 207-23.
44. Kahn, J.D., E. Yun, and D.M. Crothers, *Detection of Localized DNA Flexibility.* Nature, 1994. **368**(6467): p. 163-166.
45. Virstedt, J., et al., *The influence of DNA stiffness upon nucleosome formation.* J Struct Biol, 2004. **148**(1): p. 66-85.
46. Chazin, W.J., et al., *Comparative NMR analysis of the decadeoxynucleotide d-(GCATTAATGC)2 and an analogue containing 2-aminoadenine.* Nucleic Acids Res, 1991. **19**(20): p. 5507-13.
47. Wang, S., et al., *The specific binding of Escherichia coli integration host factor involves both major and minor grooves of DNA.* Biochemistry, 1995. **34**(40): p. 13082-90.
48. Grandgirard, N., et al., *Impact of Topoisomerase II alpha and Spermine on the clinical outcome of children with acute lymphoblastic leukemia.* Leukemia Research, 2004. **28**(5): p. 479-486.
49. Wang, J.C., *Cellular roles of DNA topoisomerases: A molecular perspective.* Nature Reviews Molecular Cell Biology, 2002. **3**(6): p. 430-440.
50. Mcclellan, J.A., et al., *Superhelical Torsion in Cellular DNA Responds Directly to Environmental and Genetic-Factors.* Proceedings of the National Academy of Sciences of the United States of America, 1990. **87**(21): p. 8373-8377.
51. Gartenberg, M.R. and J.C. Wang, *Positive Supercoiling of DNA Greatly Diminishes Messenger-Rna Synthesis in Yeast.* Proceedings of the National Academy of Sciences of the United States of America, 1992. **89**(23): p. 11461-11465.
52. Gosule, L.C. and J.A. Schellman, *Compact Form of DNA Induced by Spermidine.* Nature, 1976. **259**(5541): p. 333-335.
53. Ha, H.C., et al., *The natural polyamine spermine functions directly as a free radical scavenger.* Proceedings of the National Academy of Sciences of the United States of America, 1998. **95**(19): p. 11140-11145.
54. Oh, T.J. and I.G. Kim, *Polyamines protect against DNA strand breaks and aid cell survival against irradiation in Escherichia coli.* Biotechnology Techniques, 1998. **12**(10): p. 755-758.
55. Tabor, H., *Protective Effect of Spermine and Other Polyamines against Heat Denaturation of Deoxyribonucleic Acid.* Biochemistry, 1962. **1**(3): p. 496-&.
56. Davis, R.H., D.R. Morris, and P. Coffino, *Sequestered End-Products and Enzyme Regulation - the Case of Ornithine Decarboxylase.* Microbiological Reviews, 1992. **56**(2): p. 280-290.
57. Feuerstein, B.G., N. Pattabiraman, and L.J. Marton, *Molecular Mechanics of the Interactions of Spermine with DNA - DNA Bending as a Result of Ligand-Binding.* Nucleic Acids Research, 1990. **18**(5): p. 1271-1282.
58. Peng, H.F. and V. Jackson, *In vitro studies on the maintenance of transcription-induced stress by histones and polyamines.* Journal of Biological Chemistry, 2000. **275**(1): p. 657-668.
59. Todd, B.A. and D.C. Rau, *Interplay of ion binding and attraction in DNA condensed by multivalent cations.* Nucleic Acids Research, 2008. **36**(2): p. 501-510.
60. Besteman, K., et al., *Role of tension and twist in single-molecule DNA condensation.* Physical Review Letters, 2007. **98**(5): p. -.

61. Koster, D.A., et al., *Cellular Strategies for Regulating DNA Supercoiling: A Single-Molecule Perspective.* Cell, 2010. **142**(4): p. 519-530.
62. Liu, L.F., *DNA Topoisomerase Poisons as Antitumor Drugs.* Annual Review of Biochemistry, 1989. **58**: p. 351-375.
63. Laponogov, I., et al., *Structural insight into the quinolone-DNA cleavage complex of type IIA topoisomerases.* Nature Structural & Molecular Biology, 2009. **16**(6): p. 667-669.
64. Schoeffler, A.J. and J.M. Berger, *DNA topoisomerases: harnessing and constraining energy to govern chromosome topology.* Q Rev Biophys, 2008. **41**(1): p. 41-101.
65. Berger, J.M., et al., *Structure and mechanism of DNA topoisomerase II.* Nature, 1996. **379**(6562): p. 225-32.
66. Roca, J. and J.C. Wang, *The capture of a DNA double helix by an ATP-dependent protein clamp: a key step in DNA transport by type II DNA topoisomerases.* Cell, 1992. **71**(5): p. 833-40.
67. Morais Cabral, J.H., et al., *Crystal structure of the breakage-reunion domain of DNA gyrase.* Nature, 1997. **388**(6645): p. 903-6.
68. Mueller-Planitz, F. and D. Herschlag, *DNA topoisomerase II selects DNA cleavage sites based on reactivity rather than binding affinity.* Nucleic Acids Res, 2007. **35**(11): p. 3764-73.
69. Swinger, K.K., et al., *Flexible DNA bending in HU-DNA cocrystal structures.* EMBO J, 2003. **22**(14): p. 3749-60.
70. Vologodskii, A.V., et al., *Mechanism of topology simplification by type II DNA topoisomerases.* Proc Natl Acad Sci U S A, 2001. **98**(6): p. 3045-9.
71. Burden, D.A. and N. Osheroff, *In vitro evolution of preferred topoisomerase II DNA cleavage sites.* J Biol Chem, 1999. **274**(8): p. 5227-35.
72. Smith, S.B., L. Finzi, and C. Bustamante, *Direct Mechanical Measurements of the Elasticity of Single DNA-Molecules by Using Magnetic Beads.* Science, 1992. **258**(5085): p. 1122-1126.
73. Lipfert, J., X.M. Hao, and N.H. Dekker, *Quantitative Modeling and Optimization of Magnetic Tweezers.* Biophysical Journal, 2009. **96**(12): p. 5040-5049.
74. Zhang, H. and J.F. Marko, *Maxwell relations for single-DNA experiments: Monitoring protein binding and double-helix torque with force-extension measurements.* Phys Rev E Stat Nonlin Soft Matter Phys, 2008. **77**(3 Pt 1): p. 031916.
75. Lipfert, J., et al., *Magnetic torque tweezers: measuring torsional stiffness in DNA and RecA-DNA filaments.* Nature Methods, 2010. **7**(12): p. 977-U54.
76. Garner, M.M. and A. Revzin, *A Gel-Electrophoresis Method for Quantifying the Binding of Proteins to Specific DNA Regions - Application to Components of the Escherichia-Coli Lactose Operon Regulatory System.* Nucleic Acids Research, 1981. **9**(13): p. 3047-3060.
77. Baker, N.M., et al., *Solution structures of DNA-bound gyrase.* Nucleic Acids Research, 2011. **39**(2): p. 755-66.
78. Chatterji, M., et al., *The additional 165 amino acids in the B protein of Escherichia coli DNA gyrase have an important role in DNA binding.* Journal of Biological Chemistry, 2000. **275**(30): p. 22888-94.
79. Schoeffler, A.J., A.P. May, and J.M. Berger, *A domain insertion in Escherichia coli GyrB adopts a novel fold that plays a critical role in gyrase function.* Nucleic Acids Res, 2010.

80. Nelson, P.C., et al., *Tethered particle motion as a diagnostic of DNA tether length.* Journal of Physical Chemistry B, 2006. **110**(34): p. 17260-17267.
81. Chatterji, M., et al., *The additional 165 amino acids in the B protein of Escherichia coli DNA gyrase have an important role in DNA binding.* Journal of Biological Chemistry, 2000. **275**(30): p. 22888-22894.
82. Manjunatha, U.H., et al., *Functional characterisation of mycobacterial DNA gyrase: an efficient decatenase.* Nucleic Acids Research, 2002. **30**(10): p. 2144-2153.
83. Strick, T.R., V. Croquette, and D. Bensimon, *Single-molecule analysis of DNA uncoiling by a type II topoisomerase.* Nature, 2000. **404**(6780): p. 901-4.
84. Goyal, S., N.C. Perkins, and C.L. Lee, *Non-linear dynamic intertwining of rods with self-contact.* International Journal of Non-Linear Mechanics, 2008. **43**(1): p. 65-73.
85. Jain, S., G. Zon, and M. Sundaralingam, *Base Only Binding of Spermine in the Deep Groove of the a-DNA Octamer D(Gtgtacac).* Biochemistry, 1989. **28**(6): p. 2360-2364.
86. Ruiz-Chica, J., et al., *Fourier transform Raman study of the structural specificities on the interaction between DNA and biogenic polyamines.* Biophysical Journal, 2001. **80**(1): p. 443-454.
87. Lankas, F., et al., *Critical effect of the N2 amino group on structure, dynamics, and elasticity of DNA polypurine tracts.* Biophysical Journal, 2002. **82**(5): p. 2592-2609.
88. Maxim Y. Sheinin, S.F., John F. Marko and Michelle D. Wang *Unwound DNA under tension: structure, elasticity and sequence-dependent behavior.* in preparation 2011.
89. Fu, H., et al., *Transition dynamics and selection of the distinct S-DNA and strand unpeeling modes of double helix overstretching.* Nucleic Acids Research, 2011. **39**(8): p. 3473-81.
90. Nollmann, M., et al., *Multiple modes of Escherichia coli DNA gyrase activity revealed by force and torque.* Nat Struct Mol Biol, 2007. **14**(4): p. 264-71.
91. Gore, J., et al., *DNA overwinds when stretched.* Nature, 2006. **442**(7104): p. 836-9.
92. McClendon, A.K., et al., *Bimodal Recognition of DNA Geometry by Human Topoisomerase II alpha: Preferential Relaxation of Positively Supercoiled DNA Requires Elements in the C-Terminal Domain.* Biochemistry, 2008. **47**(50): p. 13169-13178.